

This page is intentionally left blank.

**UNIVERSIDAD SAN FRANCISCO DE QUITO**

**Colegio de Ciencias e Ingeniería**

**Wave modelling in the Ecuadorian Pacific  
using WAVEWATCH III and SWAN**

**Jeison Ebert Sosa Moreno**

**Jesús Portilla, PhD., Director de Tesis**

Tesis de grado presentada como requisito  
para la obtención del título de Ingeniero Mecánico

Quito, octubre de 2014

Universidad San Francisco de Quito  
Colegio de Ciencias e Ingeniería

HOJA DE APROBACIÓN DE TESIS

Wave modelling in the Ecuadorian Pacific  
using WAVEWATCH III and SWAN

Jeison Ebert Sosa Moreno

Jesús Portilla, PhD.  
Director de Tesis .....

Luigi Cavaleri, PhD.  
Miembro del Comité de Tesis .....

Roberto Padilla-Hernández, PhD.  
Miembro del Comité de Tesis .....

Alfredo Valarezo, PhD.  
Director de la Carrera  
Ingeniería Mecánica .....

Ximena Córdova, PhD.  
Decana de la Escuela de Ingeniería  
Colegio de Ciencias e Ingeniería .....

Quito, octubre de 2014

Las firmas fueron escaneadas debido a que los miembros del comité pertenecen a instituciones del exterior. Roberto Padilla-Hernández trabaja actualmente en "National Oceanic and Atmospheric Administration (NOAA)", Estados Unidos. Luigi Cavaleri trabaja actualmente en "Istituto di Scienze Marine (ISMAR)", Italia. El día de la defensa de tesis se usó el sistema de videoconferencia para contar con su presencia.

Ximena Córdova, PhD.  
Decana de la Escuela de Ingeniería  
Colegio de Ciencias e Ingeniería

## ©DERECHOS DE AUTOR

Por medio del presente documento certifico que he leído la Política de Propiedad Intelectual de la Universidad San Francisco de Quito y estoy de acuerdo con su contenido, por lo que los derechos de propiedad intelectual del presente trabajo de investigación quedan sujetos a lo dispuesto en la Política.

Asimismo, autorizo a la USFQ para que realice la digitalización y publicación de este trabajo de investigación en el repositorio virtual, de conformidad a lo dispuesto en el Art. 144 de la Ley Orgánica de Educación Superior.

Firma: .....  
Nombre: Jeison Ebert Sosa Moreno  
C.I.: 0802515817  
Fecha: Quito, 17 de octubre de 2014

A mis padres  
María del Carmen y Ebert

## Acknowledgments

I express my sincere thanks to Jesús Portilla, my supervisor, for introducing me into the field of wind waves, for allowing me to work with him in related works and for helping to shape and guide this work with thoughtful and detailed comments.

I am grateful to Luigi Cavaleri for hosting at ISMAR in my visit to Venice and for the careful and instructive comments about this thesis.

My gratitude to Robert Padilla-Hernández for the detailed reviewing, and for providing valuable comments of this thesis.

Al Administrador del Sistema de Cómputo de Alto Rendimiento de la USFQ (HPC-USFQ), Javier Torres, por permitir el uso del HPC.

Al Director de la Carrera de Ingeniería Mecánica de la USFQ, Alfredo Valarezo, por el apoyo.

Gracias a mis hermanas Andrea y Arianna por las risas y consejos en el trancurso del manuscrito final.

## Resumen

Durante las últimas décadas, el estudio del oleaje ha sido un foco de atención y, consecuentemente, muchos avances han sido logrados en este campo (e.g., modelo numéricos de oleaje). Muchos de estos modelos numéricos son distribuidos bajo los términos de la Licencia Pública General de GNU (e.g., WAVEWATCH III, SWAN). El modelo numérico WAVEWATCH III particularmente ha sido implementado en varios países para predicción y simulación de oleaje, principalmente en dominios de escala oceánica. El modelo SWAN, por otro lado, es más especializado en dominios costeros y regionales. El presente trabajo se enfocó en la predicción de oleaje en el Pacífico Ecuatoriano, usando las bondades de estos dos modelos. El modelo operacional de oleaje implementado provee salidas (e.g, Altura significativa y Periodo pico) disponibles en <http://ocean.usfq.edu.ec>. Como parte de esta implementación, la influencia de la extensión de la cobertura de hielo en la Antártica fue evaluada, mostrando situaciones de gran impacto en las condiciones de oleaje en la costa Ecuatoriana. Finalmente, se estudiaron diferentes alternativas para especificar condiciones de borde para el modelo costero SWAN (i.e., constante y distribuida). Los resultados muestran que no hay mayor diferencia entre ellas para los casos estudiados. Sin embargo, se necesita más investigación para condiciones de borde más generales.



## Abstract

During the last few decades, the study of ocean waves has been a focus of attention and, consequently, many developments in this field have been achieved (e.g., numerical wave models). Many of those numerical models are distributed under the terms of the GNU General Public License (e.g., WAVEWATCH III, SWAN). The wind wave model WAVEWATCH III particularly has been widely implemented in many countries to predict and simulate wind waves, mainly in ocean scale domains. The SWAN model, on the other hand, is more specialized in regional and coastal domains. The present work is focused in the prediction of wind waves in the Ecuadorian Pacific, using the capabilities of these two models. The operational wave model implemented provides output (e.g., Significant wave height and Peak period) available at <http://ocean.usfq.edu.ec>. As part of this implementation, the influence of sea ice extent in the Antarctica was evaluated, showing situations of large impacts in the wave conditions at the Ecuadorian coast. Finally, different alternatives to specify boundary conditions for the coastal model SWAN were studied. The results shows that there is not a major difference between them for the cases studied. However, further research is needed for more general boundary conditions.

# Contents

<b>1</b>	<b>Introduction</b>	<b>13</b>
1.1	Background of wind waves . . . . .	13
1.2	Relevance and aims of this study . . . . .	14
<b>2</b>	<b>Modeling wind waves</b>	<b>16</b>
2.1	Phase resolving and phase averaging models . . . . .	16
2.2	The action balance equation . . . . .	17
2.2.1	Wind-wave interactions $\mathcal{S}_{in}$ . . . . .	18
2.2.2	Quadruplets Nonlinear interactions $\mathcal{S}_{nl}$ . . . . .	19
2.2.3	Dissipation (white-capping) $\mathcal{S}_{ds}$ . . . . .	20
2.2.4	Linear wind-input $\mathcal{S}_{ln}$ . . . . .	21
2.2.5	Bottom friction $\mathcal{S}_{bot}$ . . . . .	21
2.2.6	Depth-induced breaking $\mathcal{S}_{db}$ . . . . .	21
2.2.7	Triad wave-wave interactions $\mathcal{S}_{tr}$ . . . . .	22
2.3	Wave climate in the Ecuadorian Pacific . . . . .	22
<b>3</b>	<b>Installation instructions and additional software</b>	<b>26</b>
3.1	Compilers and libraries . . . . .	26
3.2	Installation of WAVEWATCH III 3.14 . . . . .	28
3.2.1	Compiling and Linking: <code>comp</code> and <code>link</code> files . . . . .	29
3.2.2	Selecting the wave model options: <code>switch</code> file . . . . .	31
3.3	Installation of SWAN 40.91 . . . . .	31
3.4	Additional packages . . . . .	32
3.4.1	Automated Grid Generation (Gridgen) for WAVEWATCH III . . . . .	32
3.4.2	Grid Analysis and Display System (GrADS) . . . . .	33
3.4.3	Complementary subroutines . . . . .	33
<b>4</b>	<b>Operational wave forecasting model in the Ecuadorian Pacific Ocean (OPACE)</b>	<b>34</b>
4.1	Introduction . . . . .	34
4.2	Model Setup . . . . .	35
4.2.1	Grids . . . . .	35
4.2.2	Input specifications . . . . .	36
4.2.3	Physics . . . . .	36

	10
4.3	Technical implementation aspects . . . . . 37
4.4	Output available at <a href="http://ocean.usfq.edu.ec">http://ocean.usfq.edu.ec</a> . . . . . 40
4.5	Summary, conclusions, and further work . . . . . 41
<b>5</b>	<b>Influence of Antarctic sea ice extent on the Ecuadorian wave conditions</b> . . . . . <b>43</b>
5.1	Introduction . . . . . 43
5.2	Data sources and model setup . . . . . 44
5.3	A comparison of ice coverage from NCEP and ECMWF . . . . . 44
5.4	Evaluation runs (synthetic cases) . . . . . 45
5.5	Results . . . . . 48
5.6	Conclusions . . . . . 50
<b>6</b>	<b>Wave modelling of coastal processes: Case study Gulf of Guayaquil</b> <b>51</b>
6.1	Introduction . . . . . 51
6.2	Data sources and model setup . . . . . 52
	6.2.1 Physics . . . . . 52
6.3	Boundary conditions . . . . . 54
6.4	Results . . . . . 54
6.5	Summary and conclusions . . . . . 56
<b>7</b>	<b>Summary and Conclusions</b> <b>57</b>
	<b>Bibliography</b> <b>58</b>

# List of Figures

2.1	Geographical coordinates for points: Galápagos (1°S, 93°W), Esmeraldas (2°N, 80°W) and Guayas (3°S, 82°W) . . . . .	24
2.2	Mean wave spectrum and mean occurrence probability for <i>Galapagos</i> , <i>Esmeraldas</i> and <i>Guayas</i> . The values correspond to the period (1989-2010). . . . .	25
2.2a	Mean wave spectrum for Galapagos. . . . .	25
2.2b	Mean occurrence probability for Galapagos. . . . .	25
2.2c	Mean wave spectrum for Esmeraldas. . . . .	25
2.2d	Mean occurrence probability for Esmeraldas. . . . .	25
2.2e	Mean wave spectrum for Guayas. . . . .	25
2.2f	Mean occurrence probability for Guayas. . . . .	25
4.1	Bathymetries generated by Gridgen: <i>OPACE</i> , <i>Coast</i> and <i>Galap</i> . Used in the OPACE wave system . . . . .	35
4.2	Flowchart showing the <i>Main</i> subroutine in the OPACE wave system . .	39
4.3	Flowachart of the <i>Pre-processing</i> and <i>Post-processing</i> subroutines in the OPACE wave system . . . . .	40
4.3a	Pre-processing . . . . .	40
4.3b	Post-processing . . . . .	40
4.4	Integral parameters generated in the OPACE wave system. Availables at <a href="http://ocean.usfq.edu.ec">http://ocean.usfq.edu.ec</a> . . . . .	42
4.4a	Significant wave height . . . . .	42
4.4b	Peak wave period . . . . .	42
4.4c	Time series for Significant wave height at La Libertad . . . . .	42
5.1	Comparison of sea ice concentration from NCEP and ECMWF for March 2009 . . . . .	46
5.1a	Sea ice concentration for March 1, 2009 . . . . .	46
5.1b	Sea ice concentration for March 10, 2009 . . . . .	46
5.1c	Sea ice concentration for March 20, 2009 . . . . .	46
5.1d	Sea ice concentration for March 30, 2009 . . . . .	46
5.2	Comparison of sea ice concentration from NCEP and ECMWF for July 2009 . . . . .	47
5.2a	Sea ice concentration for July 1, 2009 . . . . .	47

5.2b	Sea ice concentration for July 20, 2009 . . . . .	47
5.2c	Sea ice concentration for July 20, 2009 . . . . .	47
5.2d	Sea ice concentration for July 30, 2009 . . . . .	47
5.3	Ice coverage: Scenarios A, B corresponding to March and July . . . . .	48
5.3a	Maximum sea ice concentration for <i>March</i> . . . . .	48
5.3b	Minimum sea ice concentration for <i>March</i> . . . . .	48
5.3c	Maximum sea ice concentration for <i>July</i> . . . . .	48
5.3d	Minimum sea ice concentration for <i>July</i> . . . . .	48
5.4	Significant wave height and mean period evaluated for the Coast grid .	49
5.5	Significant wave height and mean period evaluated for the Galap grid .	50
6.1	Bathymetry of the study area, Gulf of Guayaquil, resolution: 1' . . . . .	53
6.1a	Vertical scale adapted to show deep water areas' (UTM Coordinates) . . . . .	53
6.1b	Vertical scale adapted to show shallow water areas' . . . . .	53
6.2	Wave field for a specific date using both approaches Constant and Distributed (UTM Coordinates) . . . . .	54
6.2a	$H_{m,0}$ using <i>constant</i> boundary conditions . . . . .	54
6.2b	$H_{m,0}$ using <i>distributed</i> boundary conditions . . . . .	54
6.3	Comparison of the WAVEWATCH III run, <i>distributed</i> approach, with the ERA Interim ECMWF data. . . . .	55
6.4	Differences in terms of $R^2$ and $RMSE$ evaluated for August 2009 (UTM Coordinates) . . . . .	55
6.4a	$R^2$ . . . . .	55
6.4b	$RMSE$ . . . . .	55

# Chapter 1

## Introduction

### 1.1 Background of wind waves

The study of wind waves have deserved major interest during the last 65 years and its development has been steadily progressive. An important milestone was triggered during the World War II when Sverdrup and Munk (1946, 1947) were called to predict wave conditions for landing operation during the D-Day invasion in Normandy, France in 1944. Later, in order to better understand the behavior of the ocean waves, the concept of wave spectrum was introduced by Pierson (1952). Sooner, in 1960's the first-generation of numerical wave models were developed assuming the existence of a universal saturation level (Phillips, 1958). These models were still limited in the representation of all wave processes. Several new experiments and developments increased our understanding on wave growth (Mitsuyasu, 1968, 1969; Hasselmann et al., 1973) and direct measurements of wind input to waves (Snyder et al., 1981; Hasselmann et al., 1986), which led to the so called second-generation models which attempted to represent properly the overshoot phenomenon and the dependence of the high-frequency region of the spectrum on the low frequencies (Komen et al., 1994). Nevertheless, restrictions resulting from the non-linear transfer parametrization effectively required still that the spectral shape of the wind sea spectrum to be prescribed.

Encouraged by new experimental results and developments, the wave model community thorough The Sea Waves Modeling Project (SWAMP Group, 1985) established the third-generation wave models where the source terms of the Eq. 1.1 where all explicitly parametrized and integrated in time without assumptions on spectral shape

or solutions within the prognostic part of the spectrum. These improvements were possible thanks to the inexpensive parametrization of the non-linear interactions  $S_{nl}$  known as the Discrete Interaction Approximation DIA (Hasselmann et al., 1985) and development of the first third-generation model by the Wave Model Group (WAMDI Group, 1988; Komen et al., 1994) called WAM. Since then, many others wave models initially based on the WAM model, have appeared, being the most notable SWAN (Booij, Ris, & Holthuijsen, 1999) and WAVEWATCH III (Tolman, 1991, 2009).

$$\frac{DF}{Dt} = S_{in} + S_{nl} + S_{ds} + \dots \quad (1.1)$$

$F$  is the two-dimensional variance density spectrum, and the terms in the right hand represent the source terms for wind input, non-linear interactions, and dissipation, respectively.

Recent progress in understanding the physics of wave growth is given by the WISE Group (2007) and the current project NOPP (Tolman et al., 2013) which attempts to improve wind wave predictions.

## 1.2 Relevance and aims of this study

Covering more than 70% of the Earth, water constitutes an important value for our society. Since ancient times, the ocean has been used as source of food, transportation and as source of several minerals. Additionally, the ocean is a complex and fragile ecosystem which can be affected by human activities with irreversible changes. Erosion problems could wipe out beaches in a matter of few years. In addition, the interaction with the coastal zone is under increasing pressure from world's population. Economic, transport and food activities are carried out in the coastal zone, which is very challenging to manage in the correct way without affecting the environment. For these reasons, understanding the ocean behavior should be one of the main tasks in any government agenda.

In this context, the present work has as general aim to understand the use of wind wave models (e.g., WAVEWATCH III, SWAN) and the coupling procedures between them. This aim was achieved through some specific goals: **(1)** The implementation of an operational wave forecasting system in the Ecuadorian Pacific Ocean based on

the WAVEWATCH III wave model (Chapter 3, and 4). **(2)** Studying the influence of the Antarctic sea ice extent on the Ecuadorian wave conditions (Chapter 5). **(3)** Implementing the regional scale wave model SWAN in the Gulf of Guayaquil, for which boundary conditions are supplied by a large scale model (Chapter 6). The main results and conclusions are summarized in Chapter 7.



# Chapter 2

## Modeling wind waves

### 2.1 Phase resolving and phase averaging models

There are two families of wave models as considered by Battjes (1994) and Padilla-Hernández (2002).

The phase resolving wave models describe the sea surface as a function of space and time and account for effects like refraction, diffraction, triad and quadruplets wave-wave interactions. They can include also effects like dissipation processes such as bottom friction and depth-induced breaking. These models are based on Hamiltonians equations (Miles, 1981; Radder, 1992), Boussinesq equations (Peregrine, 1967; Freilich & Guza, 1984; Madsen & Sørensen, 1992) and Mild-slope equation (Berkhoff, 1974). Despite of consider important coastal processes, the generation by wind is absent.

On the other side, the phase averaging models describe the sea surface following a spectral description. In these models two methods are used, the first one, the Lagrangian in which the wave energy contained in each spectral component propagates independently along wave rays (Cavaleri & Malanotte-Rizzoli, 1981; Collins, 1972). The second one, the Eulerian approach, in which wave evolution is formulated on a grid and every grid point has the information of the whole spectrum. The advantage of the phase averaging models using the Eulerian approach is that they can efficiently solve generation, dissipation and non-linear interaction processes.

WAVEWATCH III and SWAN both are third-generation wind wave models, phase-averaged, that use the Eulerian approach to simulate wind waves, both are the models

used in this study.

## 2.2 The action balance equation

Wave propagation is described by Eq. 2.1

$$\frac{DN}{Dt} = \frac{S}{\sigma} \quad (2.1)$$

where,  $D/Dt$  represents the total derivative and  $S$  represents the net effect of sources and sinks for the spectrum  $N$ . The Eulerian form of the balance equation Eq. 2.1 is used. The action balance equation for the spectrum  $N(k, \theta; \mathbf{x}, t)$  is given by Eq. 2.2

$$\frac{\partial N}{\partial t} + \nabla_x \cdot \dot{\mathbf{x}}N + \frac{\partial}{\partial k} \dot{k}N + \frac{\partial}{\partial \theta} \dot{\theta}N = \frac{S}{\sigma} \quad (2.2)$$

$$\dot{\mathbf{x}} = \mathbf{c}_g + \mathbf{U} \quad (2.3)$$

$$\dot{k} = -\frac{\partial \sigma}{\partial d} \frac{\partial d}{\partial s} - \mathbf{k} \cdot \frac{\partial \mathbf{U}}{\partial s} \quad (2.4)$$

$$\dot{\theta} = -\frac{1}{k} \left[ \frac{\partial \sigma}{\partial d} \frac{\partial d}{\partial m} - \mathbf{k} \cdot \frac{\partial \mathbf{U}}{\partial m} \right] \quad (2.5)$$

where  $\mathbf{c}_g$  is given by  $c_g$  and  $\theta$ ,  $s$  is a coordinate in the direction  $\theta$  and  $m$  is coordinate perpendicular to  $s$ . Eq. 2.2 is valid for a Cartesian grid. The reader is referred to Komen et al. (1994); Young (1999); Janssen (2004); Holthuijsen (2007) for the demonstration and further details.

In spherical coordinates the action balance equation takes the form given by Eq. 2.6

$$\frac{\partial N}{\partial t} + \frac{1}{\cos \phi} \frac{\partial}{\partial \phi} \dot{\phi} N \cos \theta + \frac{\partial}{\partial \lambda} \dot{\lambda} N + \frac{\partial}{\partial k} \dot{k} N + \frac{\partial}{\partial \theta} \dot{\theta}_g N = \frac{S}{\sigma} \quad (2.6)$$

$$\dot{\phi} = \frac{c_g \cos \theta + U_\phi}{R} \quad (2.7)$$

$$\dot{\lambda} = \frac{c_g \sin \theta + U_\lambda}{R \cos \phi} \quad (2.8)$$

$$\dot{\theta}_g = \dot{\theta} - \frac{c_g \tan \phi \cos \theta}{R} \quad (2.9)$$

where  $R$  is the radius of the Earth,  $U_\phi$  and  $U_\lambda$  are the current components and  $c_g$  is the group velocity. In deep waters, the net source function  $S$  is generally considered

to consist of three parts, a wind-wave interaction term  $S_{in}$ , a non-linear wave-wave interactions term  $S_{nl}$  and a dissipation (white-capping) term  $S_{ds}$ . In some cases linear wind-input  $S_{ln}$  can also be considered. In shallow waters, additional processes have to be considered, most notably wave-bottom interactions  $S_{bot}$ . In extremely shallow water, depth-induced breaking  $S_{db}$  and triad wave-wave interactions  $S_{tr}$  become also important. So that the net source function is defined by Eq. 2.10

$$S = S_{ln} + S_{in} + S_{nl} + S_{ds} + S_{bot} + S_{db} + S_{tr} \quad (2.10)$$

Models solve the action balance equation but when there are not currents then the action balance equation is equivalent to the energy balance equation (Komen et al., 1994). The source terms then become  $\mathcal{S} \equiv S/\sigma$ , emphasizing the expressions that are used in the SWAN and WAVEWATCH III models.

### 2.2.1 Wind-wave interactions $\mathcal{S}_{in}$

The source term reads (Janssen, 2004)

$$\mathcal{S}_{in}(k, \theta) = \frac{\rho_a}{\rho_w} \frac{\beta_{max}}{\kappa^2} e^Z Z^4 \left( \frac{u'_*}{C} + z_\alpha \right)^2 \cos^{p_{in}}(\theta - \theta_u) \sigma N(k, \theta) + S_{out}(k, \theta) \quad (2.11)$$

where  $\rho_a$  and  $\rho_w$  are the air and water densities,  $\beta_{max}$  is a non-dimensional growth parameter,  $\kappa$  is the von Kármán' constant, and  $p_{in}$  is a constant that controls the directional distribution of  $\mathcal{S}_{in}$ .  $Z$  is defined as

$$Z = \log(kz_1) + \kappa[\cos(\theta - \theta_u)(u'_*/C + z_\alpha)] \quad (2.12)$$

where  $z_1$  is a roughness length modified by the wave-supported stress  $\tau_w$ , and  $z_\alpha$  is a wave age tuning parameter. The roughness parameter  $z_1$  is defined as,

$$U_{10} = \frac{u'_*}{\kappa} \log \left( \frac{z_u}{z_1} \right) \quad (2.13)$$

$$z_1 = \alpha_0 \frac{\tau}{\sqrt{1 - \tau_w/\tau}} \quad (2.14)$$

where  $\tau = (u'_*)^2$ , and  $z_u$  is the height at which the wind is specified. The last term considers the linear damping of swells

$$S_{out}(k, \theta) = 2s_1\kappa\frac{\rho_a}{\rho_w}\left(\frac{u'_*}{C}\right)^2\left[\cos(\theta - \theta_u) - \frac{\kappa C}{u'_*\log(kz_0)}\right] \quad (2.15)$$

where  $s_1$  is set to 1 when the damping is used and 0 otherwise. The wind friction velocity  $u'_*(k)$  includes a correction to reduce the drag coefficient at high winds (Ardhuin et al., 2010) and is defined for each frequency as

$$(u'_*)^2 = \left|u_*^2(\cos\theta_u, \sin\theta_u) - |s_u|\int_0^k\int_0^{2\pi}\frac{S_{in}(k', \theta)}{C}(\cos\theta, \sin\theta)dk'd\theta\right| \quad (2.16)$$

where the sheltering coefficient  $|s_u| \approx 1$  can be used to tune the stress at high winds.

### 2.2.2 Quadruplets Nonlinear interactions $S_{nl}$

The source term uses the Discrete Interaction Approximation DIA of Hasselmann et al. (1985) which considers a parametrisation developed for the traditional frequency-direction spectrum  $F(f_r, \theta)$ . In this model, resonant non-linear interactions occur between four wave components (quadruplets)  $\mathbf{k}_1$  through  $\mathbf{k}_4$ . It is assumed that  $\mathbf{k}_1 = \mathbf{k}_2$  therefore resonance conditions require that

$$\begin{cases} \mathbf{k}_1 + \mathbf{k}_2 & = \mathbf{k}_3 + \mathbf{k}_4 \\ \sigma_2 & = \sigma_1 \\ \sigma_3 & = (1 + \lambda_{nl}\sigma_1) \\ \sigma_4 & = (1 - \lambda_{nl}\sigma_1) \end{cases} \quad (2.17)$$

where  $\lambda_{nl}$  is a constant. The contribution  $\delta S_{nl}$  to the interaction for each discrete  $(f_r, \theta)$  combination of the spectrum corresponding to  $\mathbf{k}_1$ , is calculated as

$$\begin{pmatrix} \delta S_{nl,1} \\ \delta S_{nl,3} \\ \delta S_{nl,4} \end{pmatrix} = D \begin{pmatrix} -2 \\ 1 \\ 1 \end{pmatrix} C_g^{-4} f_{r,1}^{11} \times \left[ F_1^2 \left( \frac{F_3}{(1 + \lambda_{nl})^4} + \frac{F_4}{(1 - \lambda_{nl})^4} \right) - \frac{2F_1 F_3 F_4}{(1 - \lambda_{nl}^2)^4} \right] \quad (2.18)$$

where  $F_1 = F(f_{r,1}, \theta_1)$  etc. and  $\delta S_{nl,1} = \delta S_{nl}(f_{r,1}, \theta_1)$  etc.  $C$  is a numerical constant and  $D$  is a scaling factor to account for limited water depth.

### 2.2.3 Dissipation (white-capping) $\mathcal{S}_{ds}$

The dissipation term is defined as the sum of the saturation-based term and a cumulative breaking term  $\mathcal{S}_{bk,cu}$  (Ardhuin et al., 2010)

$$\mathcal{S}_{ds}(k, \theta) = \sigma \frac{C_{ds}^{sat}}{B_r^2} [\delta_d \max\{B(k) - B_r, 0\}^2 \quad (2.19)$$

$$+ (1 - \delta_d) \max\{B'(k, \theta) - B_r, 0\}^2] N(k, \theta) \quad (2.20)$$

$$+ \mathcal{S}_{bk,cu}(k, \theta) + \mathcal{S}_{turb}(k, \theta)$$

where

$$B(k) = \max\{B'(k, \theta), \theta \in [0, 2\pi]\} \quad (2.21)$$

$C_{ds}^{sat}$  is the saturation dissipation coefficient,  $B_r$  threshold for saturation. The combination of an isotropic part (the term that multiplies  $\delta_d$ ) and a direction-dependent part (the term with  $1 - \delta_d$ ) was intended to allow some control of the directional spread in resulting spectra. The cumulative breaking term  $\mathcal{S}_{bk,cu}$  represents the smoothing of the surface by bug breakers with celerity  $C'$  that wipe out smaller waves of phase speed  $C$ . The cumulative breaking term  $\mathcal{S}_{bk,cu}(k, \theta)$  is defined as:

$$\mathcal{S}_{bk,cu}(k, \theta) = \frac{-14.2 C_{cu}}{\pi^2} N(k, \theta) \quad (2.22)$$

$$\int_0^{r_{cu}^2 k} \int_0^{2\pi} \max\left\{\sqrt{B(f', \theta')} - \sqrt{B_r}, 0\right\}^2 d\theta' dk'$$

$r_{cu}$  defines the maximum ratio of the frequencies of long waves that will wipe out short waves.  $C_{cu}$  is a tuning coefficient expected to be of order 1. The wave turbulence interaction term of Teixeira and Belcher (2002) and Ardhuin and Jenkins (2006) is defined as:

$$\mathcal{S}_{turb}(k, \theta) = -2C_{turb} \sigma \cos(\theta_u, \theta) k \frac{\rho u_*^2}{g \rho_w} N(k, \theta) \quad (2.23)$$

where, the coefficient  $C_{turb}$  is of order 1 and can be used to adjust for ocean stratification and wave groupiness.

### 2.2.4 Linear wind-input $\mathcal{S}_{ln}$

A linear input source term is useful to allow the model to start without initial wave energy. The linear growth can be described using the formulation of Cavaleri and Malanotte-Rizzoli (1981), with a filter for low-frequency energy as introduced by Tolman (1992)

$$\mathcal{S}_{ln}(k, \theta) = 80 \left( \frac{\rho_a}{\rho_w} \right)^2 g^{-2} k^{-1} \max[0, u_* \cos(\theta - \theta_w)]^4 G \quad (2.24)$$

$$G = \exp \left[ - \left( \frac{f}{f_{filt}} \right)^{-4} \right] \quad (2.25)$$

where  $\rho_a$  and  $\rho_w$  are densities of air and water respectively.  $G$  represent a filter function.

### 2.2.5 Bottom friction $\mathcal{S}_{bot}$

The source term proposed by the JONSWAP Experiment (Hasselmann et al., 1973) is expressed in the following form:

$$\mathcal{S}_{bot} = 2\Gamma \frac{n - 0.5}{gd} N(k, \theta) \quad (2.26)$$

where  $\Gamma$  is an empirical constant, which is estimated as  $\Gamma = -0.038[m^2s^{-3}]$  for swell and  $\Gamma = -0.067[m^2s^{-3}]$  for wind seas (Bouws & Komen, 1983).  $n$  is the ratio of phase velocity to group velocity.

### 2.2.6 Depth-induced breaking $\mathcal{S}_{db}$

Eldeberky and Battjes (1996) formulate a spectral version of the bore model of Battjes and Janssen (1978), which conserves the spectral shape. Expanding their expression to include directions, the expression that is used is

$$\mathcal{S}_{db}(k, \theta) = \alpha \frac{\delta}{E} F(k, \theta) = -0.25\alpha Q_b f_m \frac{H_{max}^2}{E} F(k, \theta) \quad (2.27)$$

where  $Q_b$  is the fraction of breaking waves,  $E$  is the total spectral energy and  $\alpha = 1$  is a tunable coefficient.

### 2.2.7 Triad wave-wave interactions $\mathcal{S}_{tr}$

The Lumped Triad Approximation (LTA) of Eldeberky (1996) is expressed as

$$S_{nl3}(\sigma, \theta) = S_{nl3}^-(\sigma, \theta) + S_{nl3}^+(\sigma, \theta) \quad (2.28)$$

$$S_{nl3}^+(\sigma, \theta) = \max [0, \alpha_{EB} 2\pi c c_g J^2 |\sin \beta| \{E^2(\sigma/2, \theta) - 2E(\sigma/2, \theta)E(\sigma, \theta)\}]$$

$$S_{nl3}^-(\sigma, \theta) = -2S_{nl3}^+(2\sigma, \theta) \quad (2.29)$$

in which  $\alpha_{EB}$  is a tunable proportionality coefficient. The bi-phase  $\beta$  is approximated with the Ursell number  $U_r$ :

$$U_r = \frac{g}{8\sqrt{2}\pi^2} \frac{H_s T_{m01}^2}{d^2} \quad (2.30)$$

The triad wave-wave interactions are calculated only for  $0 \leq U_r \leq 1$ . The interaction coefficient  $J$  is taken from Madsen and Sørensen (1993):

$$J = \frac{k_{\sigma/2}^2 (gd + 2c_{\sigma/2}^2)}{k_{\sigma} d (gd + \frac{2}{15}gd^3k_{\sigma}^2 - \frac{2}{5}\sigma^2d^2)} \quad (2.31)$$

## 2.3 Wave climate in the Ecuadorian Pacific

The wave climate for the Ecuadorian Pacific has been investigated in the last years. Portilla (2011) presented detailed information about the wave conditions for three locations in deep waters, the study was based on statistics applied to the frequency-direction spectrum for locations at: Galápagos Islands, Esmeraldas and Guayas. Additionally, Portilla et al. (2013) presented an evaluation of wave power for the Ecuadorian region.

In this section, a statistical analysis applied to the frequency-direction spectrum of three locations is presented. The geographical coordinates of these points are: Galápagos (1°S, 93°W), Esmeraldas (2°N, 80°W) and Guayas (3°S, 82°W). All of these points are located at water depths larger than 3000 m (Fig. 2.1). Fig. 2.2a, 2.2c, 2.2e present the mean wave spectrum for the three locations. In these graphics, the nautical convention is used and the direction indicate where waves are going to, measured clockwise from geographic North.

According to these indicators, it is possible to say that the wave climate in the

Ecuadorian Region is characterized by four main wave regimes. Two of them propagate northwards, two southwards, all with swell characteristics. The predominant system propagates towards  $30^\circ$  (from Southwest), for this system the mean peak frequency is about 0.07 Hz. This information suggests that the Ecuadorian wave conditions are dominated by systems generated in the South Hemisphere (Portilla, 2012). The second system flows to  $130^\circ$  (from Northwest), for this system the mean peak frequency is about 0.07 Hz. The third system is the broadest and most related to local wind conditions, it is originated in the South. For Galapagos this system propagates with a direction of  $345^\circ$  and a mean peak frequency of 0.13 Hz, for Esmeraldas with direction of  $35^\circ$  and mean peak frequency of 0.17 Hz, and for Guayas with a direction of  $5^\circ$  and mean peak frequency of 0.15 Hz. The fourth system coming from the North; for Galapagos this system has a direction of  $180^\circ$  and frequency of 0.1 Hz; for Esmeraldas a direction of  $180^\circ$  and frequency of 0.15 Hz. It should be emphasized that Guayas do not present the fourth system in the spectrum.

The previously identified swells systems can also be appreciated in the mean occurrence probability plots (Fig. 2.2b, 2.2d and 2.2f). In these plots the reader can see that the fourth system (coming from the North) is one of the most weakest in terms of occurrence, but it is not in magnitude (Energy content 2D spectrum). For Guayas this system does not appear (although it was present in the occurrence plot). This information suggests that the system arrives very attenuated towards the Guayas zone. For Esmeraldas this system appears with a probability of occurrence of 35% which is relatively low. This suggests that this system could be associated with extreme events. For Galapagos, this system is well presented in magnitude and occurrence.

Wind-sea characteristics are also observed. From the energy content plots (Fig. 2.2a, 2.2c, 2.2e) clearly the swell characteristics were marked in all systems. However, for the probability occurrence plot (Fig. 2.2b, 2.2d and 2.2f), the occurrence of wind-sea conditions is not clear. For Galapagos it is noted that a significant contribution of wind-sea is in direction of  $330^\circ$  and for Esmeraldas this directions are between  $30^\circ$  and  $60^\circ$ . For Guayas the directions are between  $0^\circ$  and  $30^\circ$ .

Another important aspect to take into account is that both systems coming from the South and the system coming from the Northwest show the same occurrence levels in the three points. Additionally, the system coming from the North is the most regular.

For the Northwesterly system, the occurrence level in Esmeraldas is quite different



than in Galpagos and Guayas. It is characterized by a dispersion in frequency rather than in direction, this indicates that the generation zones are found in reduced frequencies, but from different distances. For Guayas, it is possible that the Galapagos Islands are blocking part of the energy of this system. This idea is also perceptible from spatial maps.

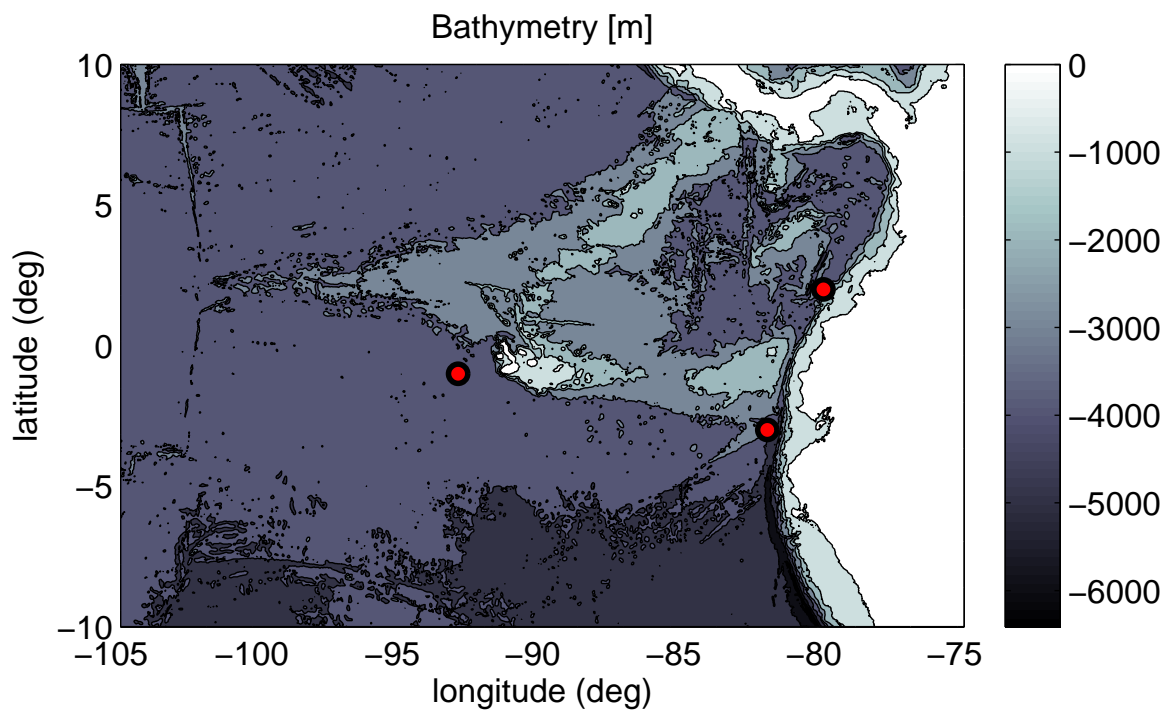
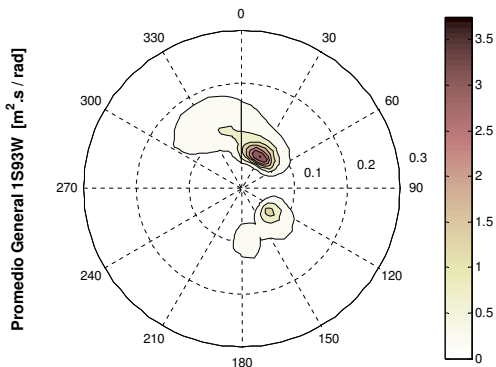
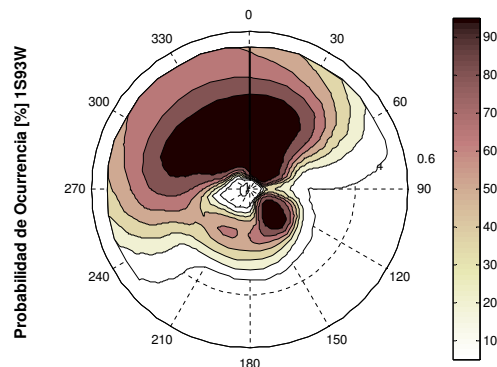


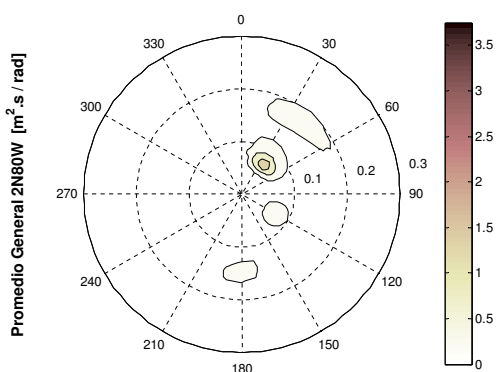
Figure 2.1: Geographical coordinates for points: Galápagos (1°S, 93°W), Esmeraldas (2°N, 80°W) and Guayas (3°S, 82°W)



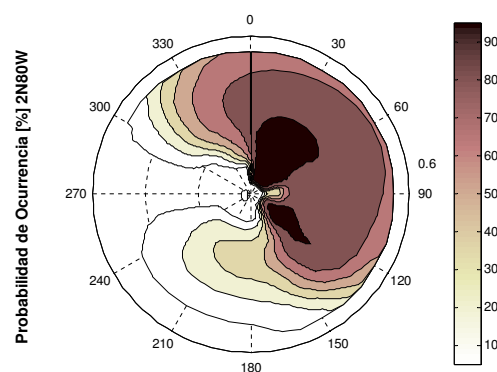
(a) Mean wave spectrum for Galapagos.



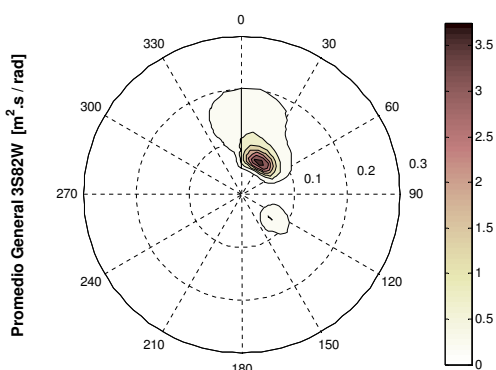
(b) Mean occurrence probability for Galapagos.



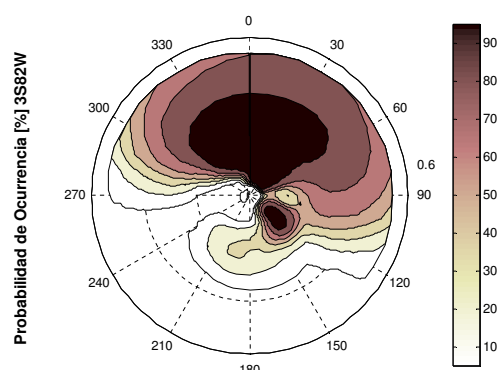
(c) Mean wave spectrum for Esmeraldas.



(d) Mean occurrence probability for Esmeraldas.



(e) Mean wave spectrum for Guayas.



(f) Mean occurrence probability for Guayas.

Figure 2.2: Mean wave spectrum and mean occurrence probability for *Galapagos*, *Esmeraldas* and *Guayas*. The values correspond to the period (1989-2010).

# Chapter 3

## Installation instructions and additional software

The WAVEWATCH III and SWAN models were implemented in the High Performance Computer of the USFQ (HPC-USFQ) and in a personal computer, respectively. The description given here is for a system Quad-Core AMD Opteron™ Processor 2378 2.4 GHz 64-Bit Architecture. 8GB of RAM distributed in 2 slots, each of one type DDR2 and 667 MHz of speed. The operating system is a UNIX/Linux distribution: Ubuntu 10.04. Nevertheless, this guide can be used to install these models in similar systems, including High Performance Computer systems. For the installation of WAVEWATCH III, it is advised to follow the user manual (Tolman, 2009), as primary source. In the following, more details are given about specific issues, such as the installation of libraries and compilers.

### 3.1 Compilers and libraries

WAVEWATCH III is written in standard FORTRAN 90. In order to make executables of these programs the computer based on UNIX/Linux must have a compiler for FORTRAN 90. In our case we install the non-commercial Intel® Fortran Composer XE 2013 which include the Intel® Fortran Compiler (`ifort`). Additionally some packages required by `ifort` are installed.

1. First of all we have to install JAVA, this can be installed in a easy way via the

terminal and the apt-get package.

```
sudo apt-get install default-jre
sudo apt-get install default-jdk
```

2. Some packages are required by ifort: gcc, build-essential, libc6-dev, ia32-libs, g++-multilib, libc6-dev-i386, alien and rpm, fort77. These packages can be installed through a Terminal via apt-get. Sometimes these packages are updated and the name could not correspond to the same name.

```
sudo apt-get install nameofpackage
```

3. The non-commercial version of ifort can be downloaded from:

```
http://www.software.intel.com
```

On the website select this package `l_fcompxe_intel64_2013.4.183.tgz`. This package must be extracted before continue with the installation process.

```
tar xvzf l_fcompxe_intel64_2013.4.183.tgz
```

The installation start by executing:

```
./install.sh
```

**NOTE:** ifort can be installed as root or local user. Choose the second one if the user do not have root permissions

4. When the installation is completed the environmental variables must be modified, in order to ifort be recognized. Edit the `.bashrc` file with GEDIT or another text editor.

```
gedit $HOME/.bashrc
```

Add this line at the end of the file:

```
source /opt/intel/bin/compilervars.sh intel64
```

Save the file.

5. The model can optionally be compiled for a distributed memory environment using the Message Passing Interface MPI, to achieve this the, the high performance message passing library openMPI (Gabriel et al., 2004) is required. openMPI can be downloaded from [www.open-mpi.org](http://www.open-mpi.org), select `openmpi-1.6.5.tar.bz2`

Create the directory structure:

```
mkdir -p $HOME/opt/openmpi
```

Extract the `openmpi-1.6.5.tar.bz2` in a temp directory

```
tar -jxf openmpi-1.6.5.tar.bz2
```

Go into the source directory

```
cd openmpi-1.6.5
```

Configure openMPI by executing

```
./configure --prefix=$HOME/opt/openmpi
```

Compile openMPI by executing

```
make -j4 all
```

```
make install
```

Edit the `.bashrc` file to add openMPI to the system path

```
gedit $HOME/.bashrc
```

Add these lines at the end of the file

```
export PATH=$HOME/opt/openmpi/bin:$PATH
export LD_LIBRARY_PATH=$HOME/opt/openmpi/bin:$LD_LIBRARY_PATH
OMPI_FC=ifort
```

## 3.2 Installation of WAVEWATCH III 3.14

In its packaged version, WAVEWATCH III 3.14 is contained in several Files:

<code>install_wwatch3</code>	Shell subroutine of WAVEWATCH III install program.
<code>wwatch3.aux.tar</code>	Compressed file with subroutines related about compiling and linking of WAVEWATCH III.
<code>wwatch3.ftn.tar</code>	Compressed file with the source code.
<code>wwatch3.tst.tar</code>	Compressed file with examples of input files.
<code>wwatch3.tst.tar</code>	Compressed file with the test cases.

1. Edit the permissions.

```
chmod 777 install_wwatch3
```

Execute the installation script

```
./install_wwatch3
```

2. At this point the install program will ask about the path installation and the temporal folder.

**NOTE:** The path installation and the temporal folder can be modified afterwards if required. The installation options are saved in `$HOME/.wwatch3.env` typing in a Terminal:

```
gedit $HOME/.wwatch3.env
```

In this file `WWATCH3_DIR` define the installation folder and `WWATCH3_TMP` define the temporal folder.

3. After the files were unpacked, 9 folders are generated.

```
aux   Raw auxiliary programs (source codes etc.).
bin   Executables and shell scripts for compiling and linking.
exe   WAVEWATCH III executables.
ftn   Source code and makefile.
inp   Input files.
mod   Module files.
obj   Object files.
test  Scripts with test cases.
work  Auxiliary work directory.
```

Locate in the `aux` folder and compile four files: `w3adc.f` `w3prnt.f` `w3list.f` `w3split.f` these files are in format FORTRAN-77, so that with `ifort` can be compiled or using the GNU Fortran 77 compiler.

```
ifort -o nameoffile nameoffile.f
```

The output files must be moved to the `bin` folder.

```
cp nameoffile <WAVEWATCH III_DIR>/bin/nameoffile
```

4. We have to set the environmental variables for WAVEWATCH III . Edit the `.bashrc` file with GEDIT or another text editor.

```
gedit $HOME/.bashrc
```

Add these lines at the end of the file:

```
export PATH=$PATH:<WAVEWATCH III_DIR>/bin
export PATH=$PATH:<WAVEWATCH III_DIR>/exe
```

Save the file.

### 3.2.1 Compiling and Linking: `comp` and `link` files

Before start the compilation of the wave model we have to modify compiling and linking options in the `bin` folder.

1. Open the `comp` file in the `bin` folder and modify sections: 2.b, 3.a and 3.d according to the computer FORTRAN-90 compiler. Do not forget that we have installed `ifort` as our F90 compiler. In the `bin` directory also exist a file `comp.mac_pro_Intel` which is a template with the configuration for `ifort`. This file can be copied and replaced by the default `compfile`.

```
cp comp.mac_pro_Intel comp
```

The `comp` file must look like this, in part 2.b:

```

1  opt="-c -g CB -list -O3 -module $path_m"
2  if [ "$name" != 'gx_outp' ] && [ "$name" != 'gx_outf' ]
3  then
4      opt="$opt -convert big_endian"
5  fi
6
7  if [ "$mpi_mod" = 'yes' ]
8  then
9      comp=mpif90
10 else
11     comp=ifort
12 fi
13
14 $comp $opt          $name.$fext > $name.out 2> $name.err
15 OK="$?"
```

In the `bin` directory also exist a file `link.mac_pro_Intel` which is template with the configuration for `ifort`. This file can be replaced by the default `link` file.

```
cp link.mac_pro_Intel link
```

The link file must look like this, in part 3:

```

1  opt="-O3 -Zp8 -tpp7 -o $prog"
2
3  if [ "$mpi_mod" = 'yes' ]
4  then
5      comp=mpif90
6  else
7      comp=ifort
8  fi
9
10 $comp $opt $objects          > link.out 2> link.err
11 OK="$?"

```

Note: Currently, the 4.18 version of WAVEWATCH III is available. This version also was also installed and tested, and the corresponding template files for compiling and linking are: `comp.gnu` and `link.gnu`

### 3.2.2 Selecting the wave model options: `switch` file

The last step is edit the `switch` file in the `bin` folder according with needs of the user. The `switch` file contains a set of strings identifying the wave model options to be selected.

```

F90 NOGRB LRB4 DIST MPI LLG PR3 FLX2 LN1 ST2 STAB2 NL1 BT1 DB1 MLIM
TR0 BS0 XX0 WNX1 WNT1 CRX1 CRT1 00 01 02 03 04 05 06 07 011 014

```

Until this point we have set the options for WAVEWATCH III , we are ready to compile the wave model.

```
w3_make
```

## 3.3 Installation of SWAN 40.91

The SWAN 40.91 can be downloaded from:

```
swanmodel.sourceforge.net/download/zip/swan4091.tar.gz
```



the source must be extracted in a folder. After that open a terminal locate into the folder and execute the next command

```
make config
```

if everything is OK no errors will appear in the terminal. If OpenMPI is installed in the computer, SWAN can be built in parallel mode executing the next command:

```
make omp
```

If OpenMPI is not installed, the user can compile the SWAN in serial mode using:

```
make ser
```

Note: Add the SWAN path to the .bashrc file, copy this line at the end of \$HOME/.bashrc file:

```
PATH=<SWAN_PATH>:$PATH
```

## 3.4 Additional packages

### 3.4.1 Automated Grid Generation (Gridgen) for WAVEWATCH III

Gridgen is an automated grid generation software package written in Matlab language, which has been developed for use with WAVEWATCH III (Tolman, 1991, 2009) by Chawla and Tolman (2007) at NCEP.

Basically, Gridgen creates obstructions grids for sub-grid modelling (Tolman, 2003). To operate Gridgen uses two types of global datasets, the high resolution 2 Arc-minute global bathymetry ETOPO2 (Gridded, 2006) and the high resolution shoreline database GSHHS (Wessel & Smith, 1996).

Gridgen comes with different modules to help users perform specific tasks. The grid generation module develops first guess low resolution grid from the high resolution bathymetry. The boundary module extracts all boundaries from the global boundary database that lie inside the design grid, properly accounting for boundaries being split by the grid domain. The land mask module generates the land-sea mask, separating the cells into 'wet' and 'dry' cells, with the help of the bathymetry and boundary data. The wet cell module groups all the wet cells that are connected together. The sub-grid module builds the obstruction grids for unresolved boundaries in the sub-grid domain.

The mask modification module modifies the final land-sea mask to separate the nodes into active, inactive and boundaries nodes.

### 3.4.2 Grid Analysis and Display System (GrADS)

GrADS is an interactive desktop tool used in many applications related to Earth sciences, it was developed by IGES (Doty, 1995). It is distributed freely under terms of the GNU Public License.

GrADS provides access, manipulation and display of Earth sciences data. It includes a 4-dimensional data model including variables like latitude, longitude, level and time. Furthermore, it uses an interpreted scripting language to give instructions for processing data. This tool includes a variety of graphical outputs for data representation like line, bar, scatter plots, contour, streamline and wind vector. Additionally, the most common formats are available to exports graphics.

GrADS has established conventions to write and read packages of information in binary format in a control file with extension `.ctl`, WAVEWATCH III uses the GrADS convention to write its outputs in this format.

### 3.4.3 Complementary subroutines

`read_grads`. Routine written in Matlab language by Sturm (2008), which reads the GrADS control file and retrieves the variables from the binary file.

# Chapter 4

## Operational wave forecasting model in the Ecuadorian Pacific Ocean (OPACE)

### 4.1 Introduction

Operational forecast systems for waves have progress significantly in recent years. This growth have been justified by the impact of waves to coastal settlements, and economic activities related to coastal and offshore activities, which are affected by extreme waves generated during intense meteorological activity. Currently, several institutes around the world are responsible for producing global forecasts (NCEP, ECMWF, METEOFRANCE, U.K. Meteorological Office). These institutes include global forecasts and also serve specific areas. Before the present implementation, in the Ecuadorian Pacific zone specifically, only low resolution wave information from such centers was available. Therefore, the lack of specific wave data and products motivated the implementation of a wave local forecasting system.

The Ecuadorian Pacific Ocean (OPACE) wave model includes a global grid (GLOBAL), one regional grid (OPACE) and two grids with finer resolution, and focusing in the Ecuadorian shore (COAST) and Galápagos Islands (GALAP) respectively. The model implemented was the third-generation spectral ocean wave model WAVEWATCH III (Tolman, 1991, 2009), which is forced with input winds, and ice coverage conditions from the NCEP's Global Forecast System, GFS (Moorthi et al., 2001).

## 4.2 Model Setup

WAVEWATCH III was implemented and adapted to the Ecuadorian Pacific Ocean (OPACE), this section includes a description of the grids, input data, and physical formulations used.

### 4.2.1 Grids

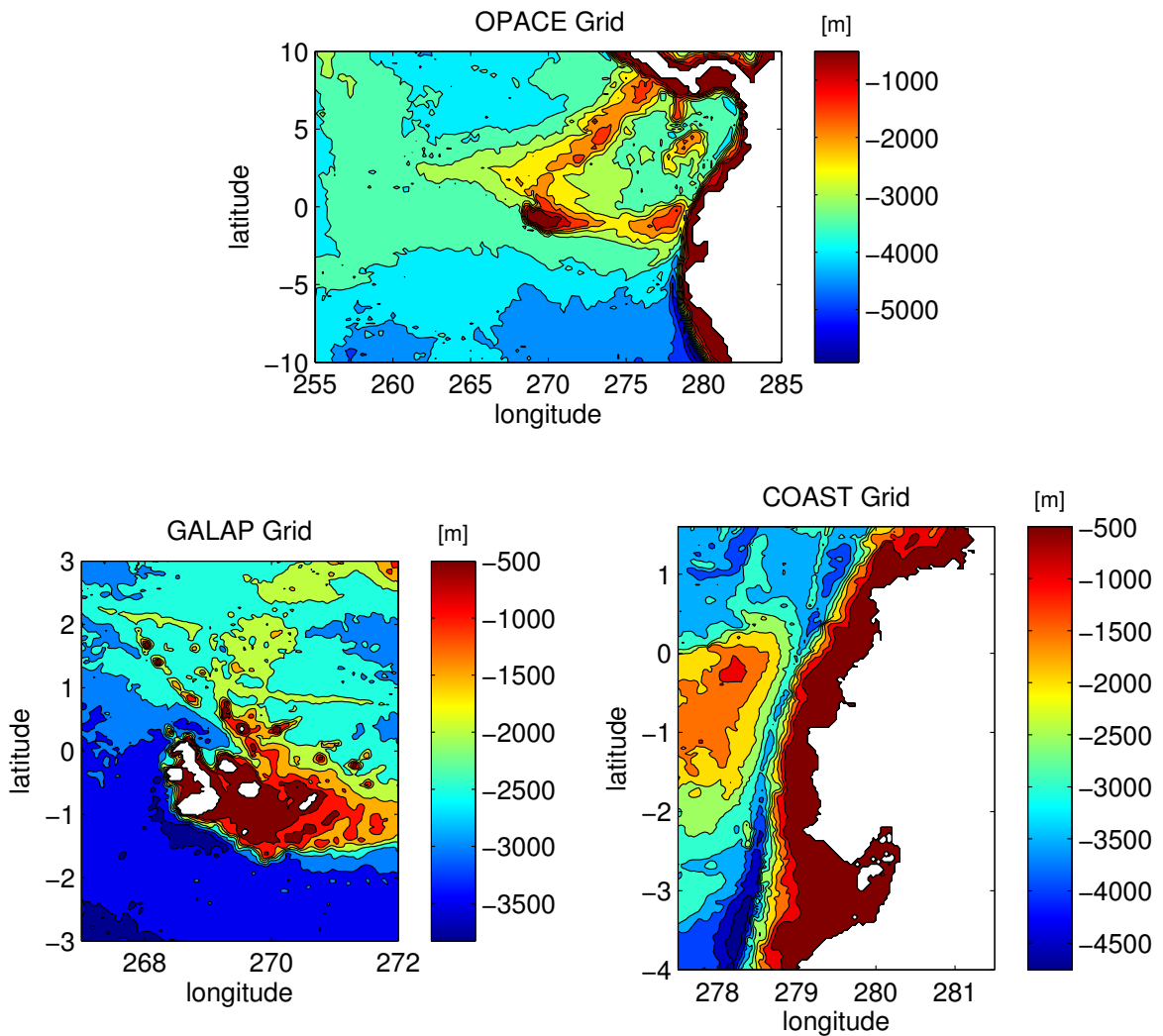


Figure 4.1: Bathymetries generated by Gridgen: *OPACE*, *Coast* and *Galap*. Used in the *OPACE* wave system

The WAVEWATCH III model can be run using a mosaic approach (Tolman, 2008),

where a set of wave model grids is converted into a single wave model by considering two-way interactions between grids. This increases computational efficiency by restricting the higher resolution grids only in interested areas. Considering this approach, WAVEWATCH III was implemented with several grids with high resolution in the Galapagos Islands and the Coastal Pacific Region.

All grids were constructed using the Automated Grid Generation (Gridgen) (Chawla & Tolman, 2007), which use the ETOPO2 bathymetry as reference grid and generate automatically: bathymetry, land-sea masks, and obstruction grids (these last account for wave attenuation by unresolved islands). The OPACE Grid has a resolution in Latitude and Longitude of  $1/4^\circ$ , and the COAST and GALAP Grids have a resolution in Latitude and Longitude of  $1/30^\circ$ . See Fig. 4.1

The spectral domain has been divided into 30 frequency and 24 directions. The range is between 0.035–0.5476 Hz, set in geometric scale. The direction was set from  $7.5^\circ$  to  $352.5^\circ$ .

## 4.2.2 Input specifications

The wave forecasting model OPACE is driven using wind fields and sea ice concentration from the Global Forecast System obtained through the NOAA National Operational Model Archive and Distribution System (NOMADS) (Rutledge et al., 2006).

The GFS model runs 4 times each day at 0000, 0600, 1200 and 1800 UTC and produces up to 192 hours forecast conditions with time steps of 3 hours. The OPACE wave model uses only the 0000 UTC results to produce forecast for the Ecuadorian Pacific.

## 4.2.3 Physics

The WAVEWATCH III packages used to run the forecasts are:

1. Wind input and dissipation from Tolman and Chalikov (1996) with stability correction.
2. Nonlinear interactions using DIA approximation (Hasselmann et al., 1985).

3. Depth-induced breaking from Battjes and Janssen (1978) with a Miche-style shallow water limiter.
4. Bottom friction from Hasselmann et al. (1973) and no bottom scattering.
5. Combined propagation scheme of QUICKEST (Leonard, 1979; Davis & Moore, 1982) with ULTIMATE TVD (Leonard, 1991), alleviation of the Garden Sprinkler Effect from Tolman (2002).

### 4.3 Technical implementation aspects

The OPACE wave model consist of several subroutines written in Matlab, Fortran, Perl and Bash language which constitute an automatic system to download the necessary input files (i.e. Wind U V and Ice Coverage), execute pre-processing tasks, run the wave model, and post-processing the output data. The system is implemented in a High Performance Computing thanks to the support of the High Performance Computing Team of the USFQ. The forecast result can be accessed freely from <http://ocean.usfq.edu.ec> where integral wave parameters like Significant wave height, and Peak wave period, are given as animated images. Additionally, time series of Significant Wave Height ( $H_{m,0}$ ), at specific locations is given.

The HPC-USFQ in the USFQ is used for research purposes in several areas like Chemistry, Physics, Weather, etc., it is operational since July, 2013. Initially the OPACE forecast system was run daily without interruptions. However, since then, the number of users has increased, and therefore, additional subroutines had to be written to deal with this issue, running the system overnight when processors are available. The OPACE forecast system became operational since September, 2013 and it has been running since then almost continuously.

A flowchart showing the MAIN subroutine for the OPACE system is showed in Fig. 4.2. The MAIN subroutine starts at 4AM (when in principle, the GFS forecast products are already available). As first tasks, the MAIN subroutine, checks if there is any previous pending JOB in the HPC's queue, if this is the case, such previous job is killed, this is to avoid redundant runs, in the case that previous runs that suffered delay are still running (the new run starts from the time when the last valid forecast finished successfully). Then, having resolved issues about previous JOBS, the MAIN

subroutine, call the Pre-processing subroutine (explained later). Then, the MAIN subroutine, assign a JOB ID in the HPC and the post-processing subroutine waits until the OPACE wave model completes the calculations. If the OPACE system is not completed until 1AM of the next day, the post-processing subroutine stops and the entire simulation is postponed to the next day at 4AM. When a JOB assigned is completed, the MAIN subroutine saves the final wave conditions to be used as initial conditions for the next day run.

The Pre-processing as well as the Post-processing subroutines are executed in a personal computer. However, the WAVEWATCH simulation run is executed in the HPC. These computers are communicated via SSH allowing the transfer files between them.

The Pre-processing subroutine Fig. 4.3a, re-format necessary input files in a format that could be read by WAVEWATCH III. Firstly, the Pre-processing subroutine, checks the date from the last initial conditions generated from a previous run and continues with the next date. After that, it downloads the GFS Wind input at 10 m height above-sea level. These files contain the U and V components with a resolution of  $0.5^\circ$  in .GRIB2 format.

Then, the Pre-processing subroutine downloads the GFS Ice cover at the Earth surface (with the same resolution  $0.5^\circ$ ), also given in .GRIB2 format. The ice coverage files are downloaded using a Perl script written by Ebisuzaki (2006) from NCEP.

At this point, Wind (U,V) and Ice cover inputs are downloaded. However, WAVEWATCH III can't read .GRIB2 files directly, therefore these input files are re-formatted in ASCII format. These .GRIB2 files are read using the free-open source Matlab toolbox: NCTOOLBOX (<http://code.google.com/p/nctoolbox/>). The files are re-formatted using the Fortran free-format 16F5.2 (which means 16 columns, 5 characters by number and 2 decimals). The files generated contain a header indicating date and time of the corresponding fields. When these files (ASCII Wind and Ice files) are ready, they are transferred to HPC in order to start the simulation run.

The simulation run takes about 1 hour and uses 16 physical processors. The initial conditions of the last two days from the current forecast day are stored in the HPC, this is good practice used in case the system fails. After the simulation run completes, the output is transferred back to the personal computer where the Post-processing subroutine is executed.

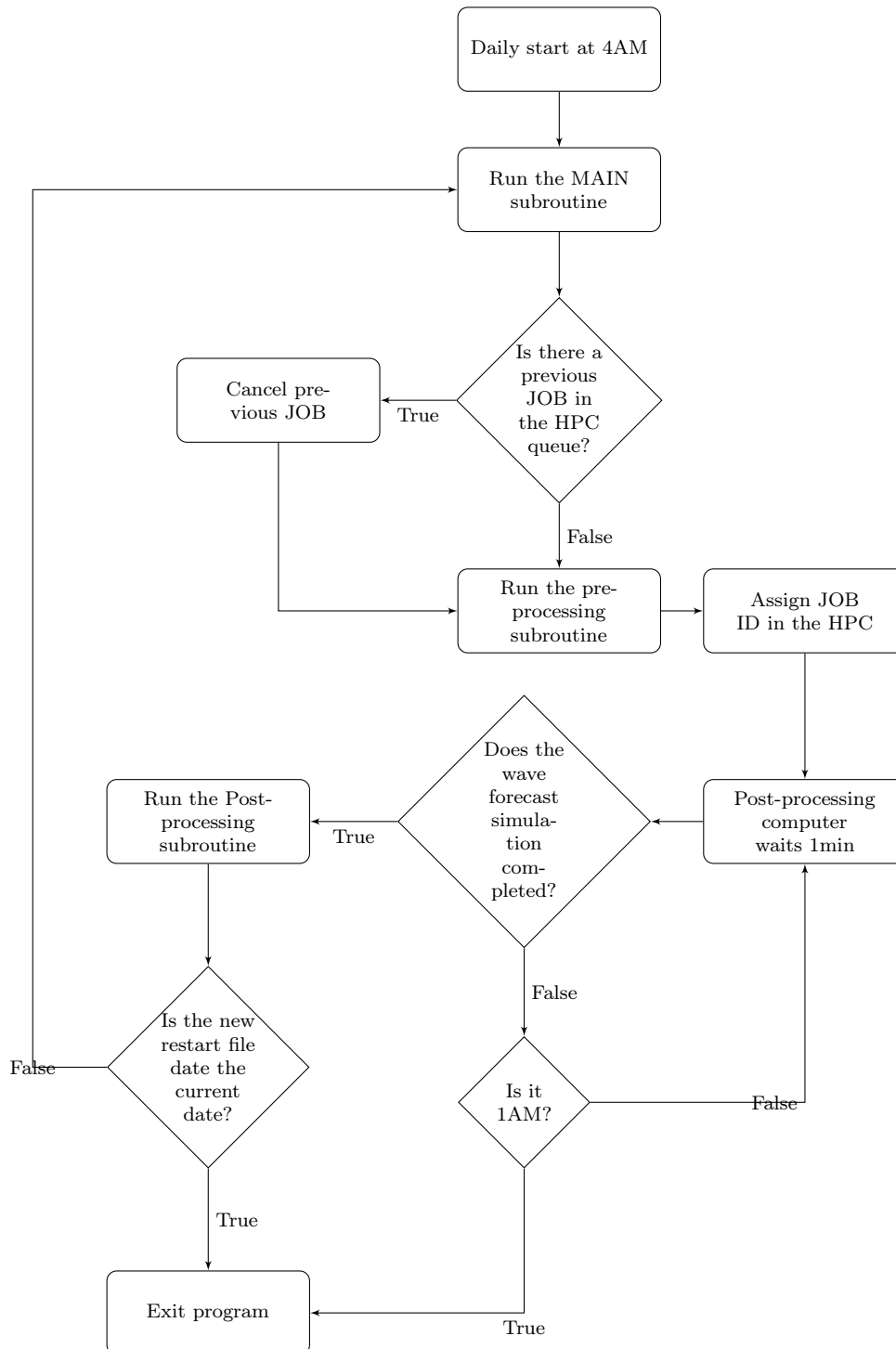


Figure 4.2: Flowchart showing the *Main* subroutine in the OPACE wave system



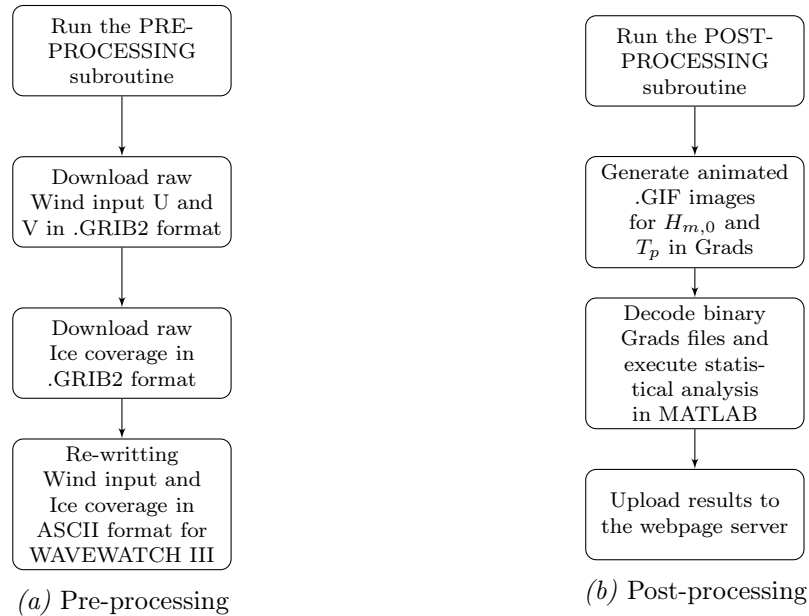


Figure 4.3: Flowachart of the *Pre-processing* and *Post-processing* subroutines in the OPACE wave system

The Post-processing subroutine is showed in Fig. 4.3b. This is executed automatically after the forecast run is completed. It includes scripts for plotting, decoding and uploading results. The output (integral parameters) in Grads binary format are read using the Grads desktop tool (Doty, 1995). Using this tool, two animated images showing the forecast are generated for both  $H_{m,0}$  and  $T_p$ . Then, the GRADS output is read to Matlab using the Sturm (2008) routine. After that, the Coastal Alert Risk System processes these results and summarizes the  $H_{m,0}$  time series with indication of possible extreme conditions. This product is printed in .PDF format. Finally, when all products are successfully obtained, the Post-processing subroutine upload all information to the web server.

## 4.4 Output available at <http://ocean.usfq.edu.ec>

The output fields of  $H_{m,0}$  and  $T_p$  are presented in Fig. 4.4. For these images, the three grids (OPACE, COAST and GALAP) were joined, the OPACE grid acts as background and the COAST and GALAP were situated over this background. These last have higher resolution, therefore zooming is possible if required.

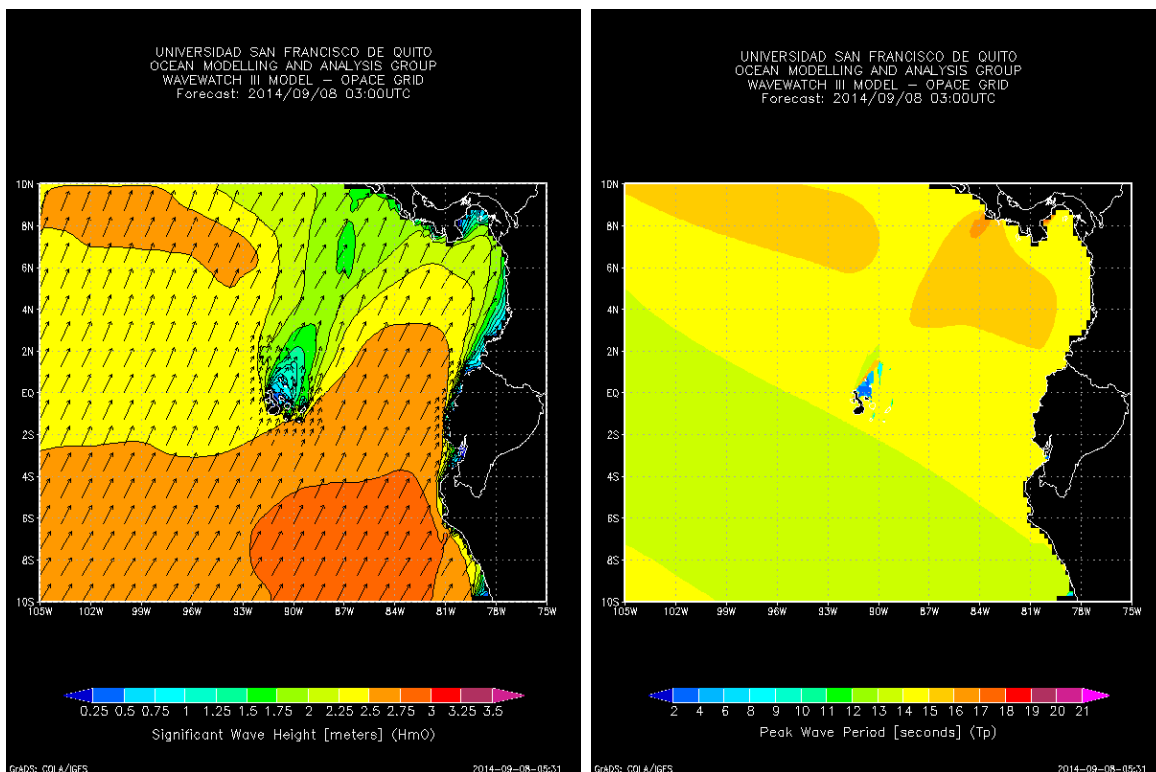
Results for the Coastal Alert Risk System are also presented in Fig. 4.4. Based on

the grid points of the COASTAL grid, the Coastal Alert Risk System generate a report for several populated places along the Ecuadorian coast, namely: Bahía de Caráquez, Esmeraldas, La Libertad, Manta, Muisne, Posorja, Puerto Bolívar, Puerto López, Isla Puná y San Lorenzo. Through this report, the idea is to provide users with a simple tool about the wave forecast. For this, the Coastal Alert Risk System uses a color bar to describe different types of wave conditions of  $H_{m,0}$ , green for normal activity, yellow for moderate activity, orange for high activity, and red for extreme events. Moderate, High and Extreme wave conditions are based on the 98th, 99th and 99.99th percentile of the 2009 year, respectively. These  $H_{m,0}$  time series are given for 8 days forecast horizon, a good period for most practical applications. Fig. 4.4 shows the color bar for wave conditions and the time series at La Libertad.

## 4.5 Summary, conclusions, and further work

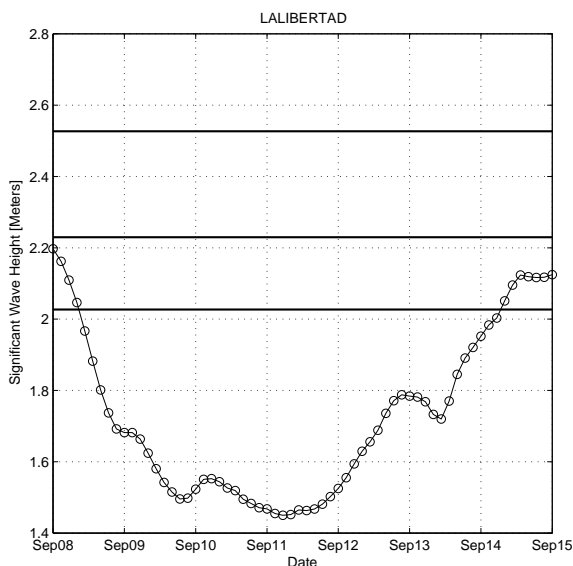
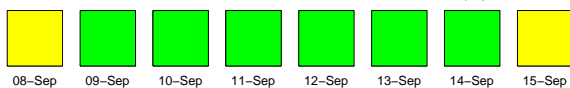
The OPACE wave forecast system was implemented in the HPC-USFQ satisfactorily and is a system that aims to produce products both for research purposes and also as a free service to the community offered by USFQ. The OPACE wave model use the third-generation model WAVEWATCH III from NOAA.

As further work, the OPACE system is to be used to generate boundary conditions for coastal applications using the SWAN model. These coastal grid products will also be accessible through the web. In addition, the statistical procedure used to characterize conditions as normal, high or extreme is to be improved.



(a) Significant wave height

(b) Peak wave period



(c) Time series for Significant wave height at La Libertad

Figure 4.4: Integral parameters generated in the OPACE wave system. Availables at <http://ocean.usfq.edu.ec>

# Chapter 5

## Influence of Antarctic sea ice extent on the Ecuadorian wave conditions

### 5.1 Introduction

The accuracy of present state-of-the-art wave models in the Southern Hemisphere is limited due to several factors, among them, the ice concentration in the Antarctic region, which under specific conditions play the role of a geographical boundary for waves in the Ecuadorian Pacific. Also from the analysis of the wave conditions in the Ecuadorian Pacific, and during the implementation of the wave forecast system (OPACE), it became apparent that the ice concentration in the Antarctica affects to some extent ocean waves in South American coasts. In relation to this, some advances (Ardhuin et al., 2011) have shown that Southern icebergs concentration affects ocean waves in the Southern Pacific, due to iceberg blocking of swells. In addition, in Portilla (2012), it was found that swells arriving to the Ecuadorian region may be generated in places as remote as the South of Australia, traveling along the Pacific Ocean, and possibly crossing the Antarctic region. Therefore, if certain conditions are met during this travel, the ice in the Antarctic region, might be in the pathway of these waves, totally blocking them or reducing its energy. For this reason, in this chapter the aim is to quantify the magnitude of such influence. Naturally, the concentration of ice in the Antarctica presents a seasonal variability, with large concentrations in the Austral winter (June-July-August), and less concentrations in other months. In addition, very long waves are typical in front of the Ecuadorian coasts in the months of March and

September, where the ice concentration reduces significantly, while the storm activity is still significant. Therefore, the methodology followed here considers two synthetic situations in which ice concentration reaches very large and very low ice concentrations levels respectively. The impact on waves is evaluated running synthetic hindcasts (with real winds but synthetic ice fields) using the WAVEWATCH III model (OPACE system).

## 5.2 Data sources and model setup

Ice coverage fields for these runs were obtained from the MMAB Sea Ice Analysis, NCEP (Grumbine, 1996). It provides a global grid ice coverage with a resolution of  $0.08^\circ$ . Another global grid ice coverage dataset was from the Era-Interim Reanalysis, ECMWF (Dee et al., 2011) with a resolution of  $0.75^\circ$ . During data pre-processing it was found that ice coverage fields differ significantly between these two sources, and because of the resolution and data consistency, the evaluation runs were carried out here using the NCEP data.

The data period of the NCEP databases covers the years from 2005 to 2011. The wind fields correspond to the ECMWF ERA-interim databases of the year 1998 with  $0.75^\circ$  of resolution.

## 5.3 A comparison of ice coverage from NCEP and ECMWF

In order to understand the differences of ice concentration between the two sources (ECMWF and NCEP), a first task consisted of a comparison between them. To illustrate these differences, in Figures 5.1 and 5.2 some comparison results are presented for the reference months March and July respectively. The year 2009 was chosen because it is a year with significant wave activity for which data from both sources is available (Portilla, 2011). The figures show the 100% ice concentration limit. The displayed region comprises from 120E and 90W, which is the area of possible influence for waves in the area of interest (Ecuadorian coasts). In Fig. 5.1 we can appreciate clearly a difference of about  $2^\circ$  in the limit of the ice sea boundary between both institutes (NCEP

has larger ice concentrations). In Fig 5.2 an increase in ice coverage, compared to March, is seen due to winter conditions. In this plot a similar difference of 2° is present (again larger for NCEP). It should be noted therefore that predicted wave conditions, in the Ecuadorian region, between these two datasets from both institutes may differ depending on the influence of this ice boundary extent.

## 5.4 Evaluation runs (synthetic cases)

Since the main purpose is to evaluate the impact of the Antarctic ice coverage as geographical boundary of waves encountered in the Ecuadorian zone, the evaluation runs consider two synthetic situations. The first is a situation with high ice concentrations. For this, the synthetic ice field is composed with the maximum ice concentration at each lat-lon bin during the data period (2005-2011), for the months of March and July respectively, Scenarios A. Correspondingly, the second situation considers the minimum value at each bin in this period and for the reference months, Scenarios B. With this scenarios, although the ice concentrations are not strictly real, they are expected to keep a high correspondence with real situations.

Wind fields on the other hand, correspond to hindcasts of the ECMWF ERA-interim, for the year 1998 (a year with high wave activity). These wind fields are used as they are, without any manipulation.

1. Scenario A-March: The maximum ice coverage of the month
2. Scenario B-March: The minimum ice coverage of the month
3. Scenario A-July: The maximum ice coverage of the month
4. Scenario B-July: The minimum ice coverage of the month

Fig. 5.3 shows the corresponding ice coverages used for the different scenarios. Correspondingly, four simulations were performed. In order to appreciate the maximum differences, integrals parameters were evaluated and obtained. Namely, significant wave height and mean wave period. For each scenario, the maximum and minimum values in the grid were obtained. The results are presented in the next section.

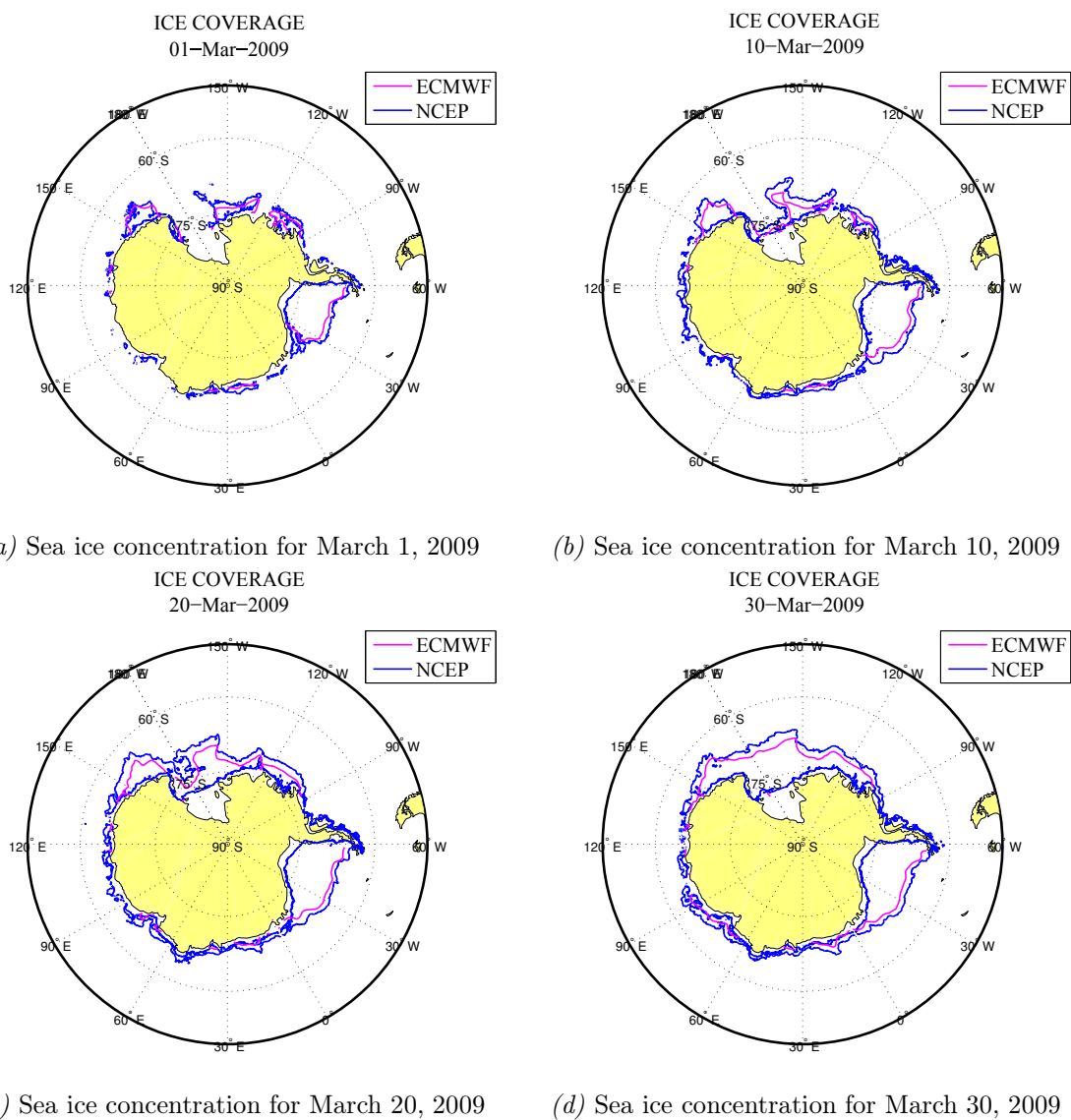


Figure 5.1: Comparison of sea ice concentration from NCEP and ECMWF for March 2009

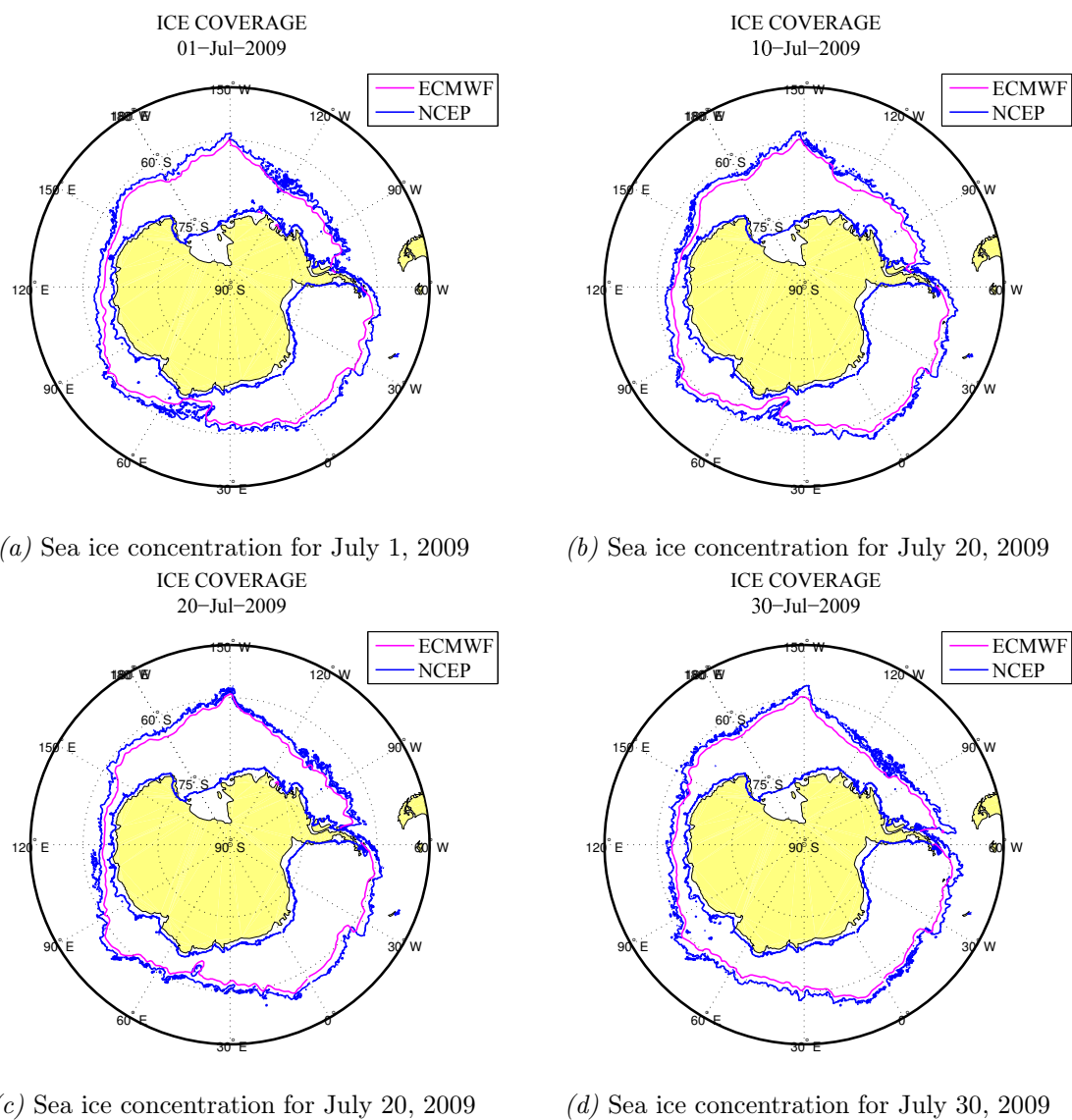


Figure 5.2: Comparison of sea ice concentration from NCEP and ECMWF for July 2009



It should be noted that in Fig. 5.1 and 5.2 a Stereographic projection of the Antarctic region is used in order to highlight the differences between the two centers, while Fig. 5.3 uses a Rectangular projection to show the ice coverage magnitudes for the different scenarios in a global scale.

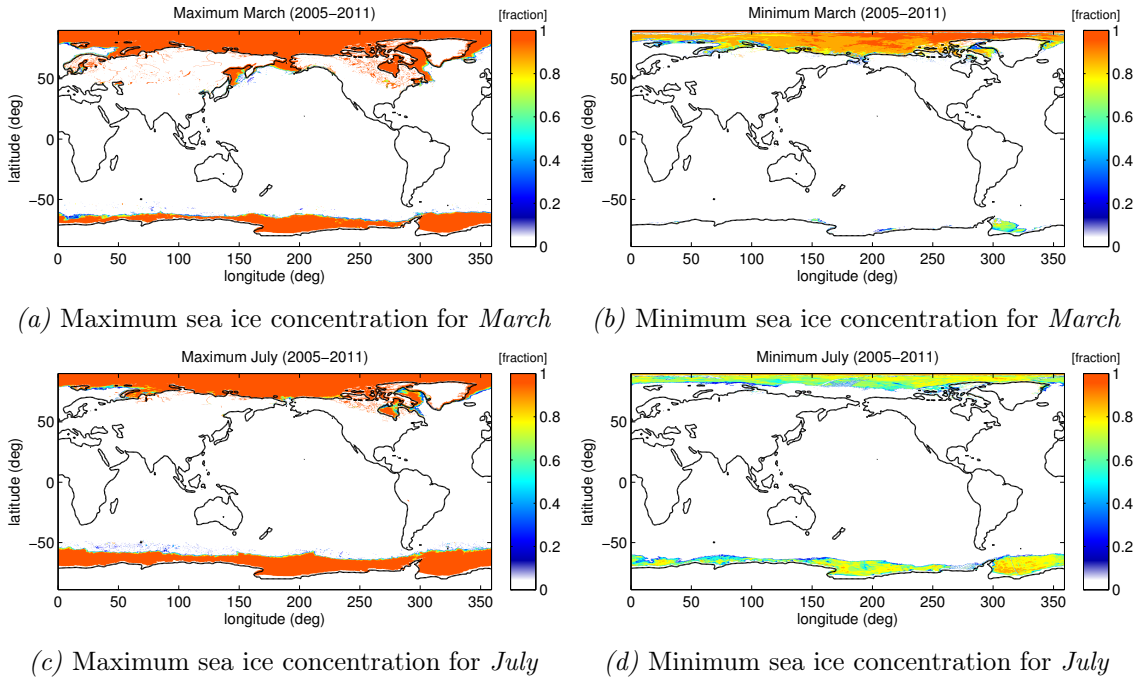


Figure 5.3: Ice coverage: Scenarios A, B corresponding to March and July

## 5.5 Results

Results for the coastal grid are shown in Fig. 5.4. In this figure, it can be appreciated that the maximum difference in March occurs in northern area and can reach values of up to 1.4m. for  $H_{m,0}$ , while in general, there is a difference of about 1m in the whole domain. In July, differences are on the order of about 1.6m, but large areas with a the maximum value of 1.8m are found. For mean wave period, in March the maximum difference is about 10s (inside the Gulf of Guayaquil), while in a large part of the grid, the difference is about 5s. In July, the differences in wave period are lower than March with a typical value of about 3s.

Additionally, results for Galap grid are shown in Fig. 5.5. It is showed that the maximum difference in March with a  $H_{m,0}$  of about 1.4m. But, in general the difference

reach 1m. In July, the  $H_{m,0}$  reach values of 1.4 as maximum, but in general the values are around 1.2m. The difference in mean wave period for both months reach 5s. the maximum occurs in July behind the Isabella Island with values about 8s. It should be noted that in July, the dominant wave conditions are from southwest, while in March a mixture of waves from southwest and northwest are typical. This can be appreciated to some extent in the wake after the islands.

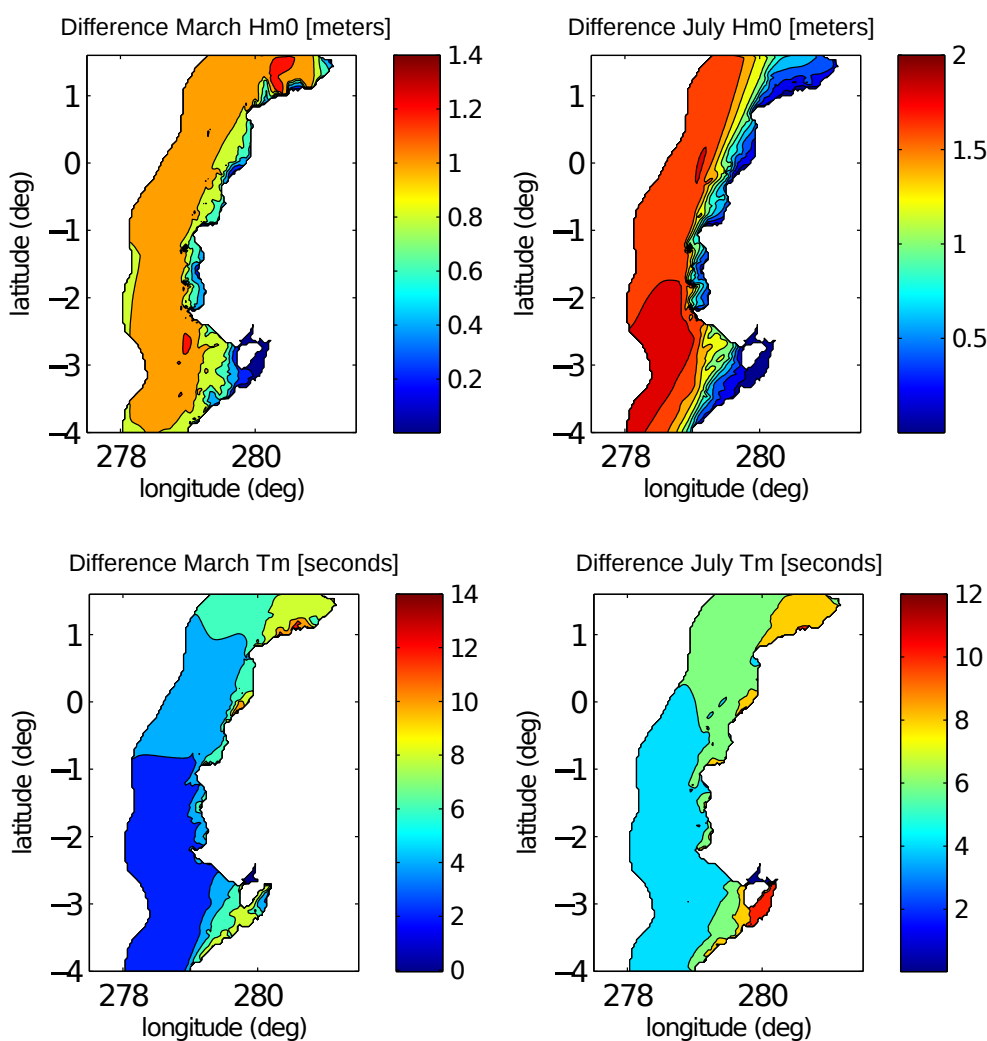


Figure 5.4: Significant wave height and mean period evaluated for the Coast grid

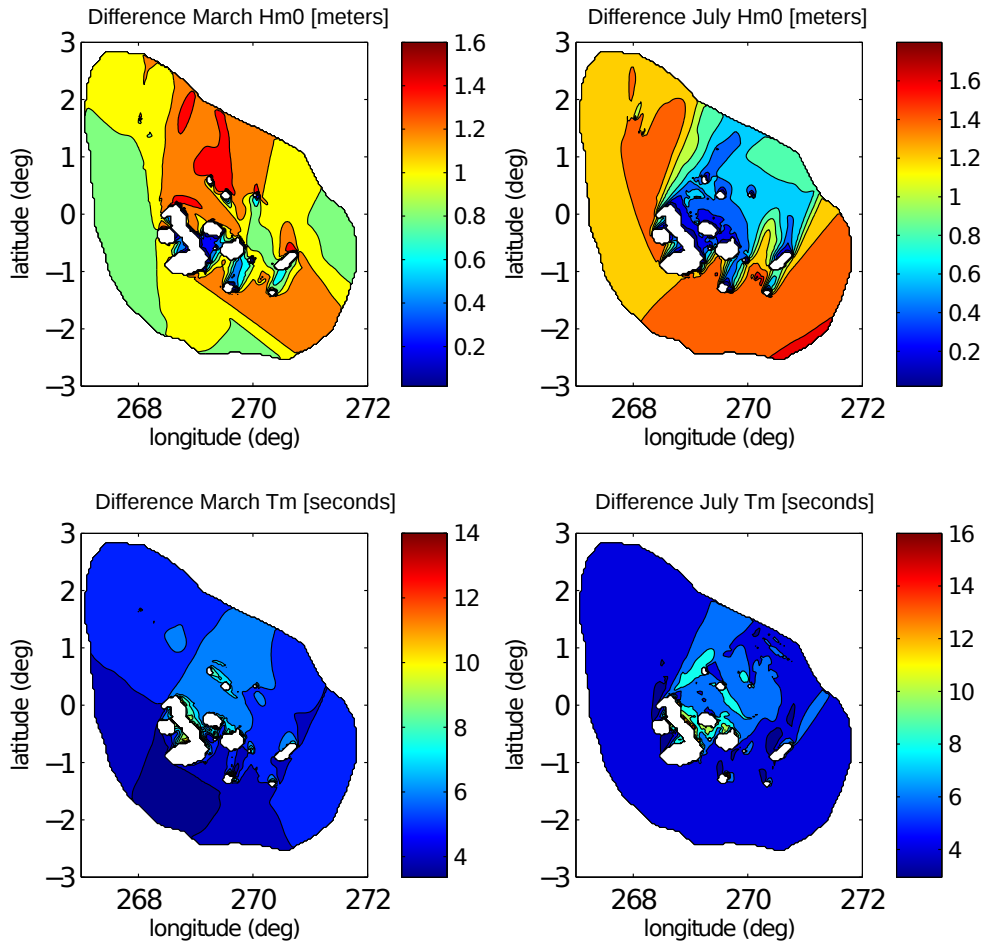


Figure 5.5: Significant wave height and mean period evaluated for the Galapagos grid

## 5.6 Conclusions

Despite of the NCEP and ECMWF ice coverage data come from the same satellite, they use different decoding algorithms to generate the ice field. This may contribute to the significantly difference between them.

From these results, we can observe that the ice coverage concentration in the Antarctica play a significant role in the wave conditions in the Ecuadorian Pacific. The runs carried out here have a preliminary character, and it is clear that a more detailed evaluation should be carried out in regard to model implementation and verification.

# Chapter 6

## Wave modelling of coastal processes: Case study Gulf of Guayaquil

### 6.1 Introduction

This chapter describes the implementation of the coastal wave model SWAN (Booij et al., 1999) in the Gulf of Guayaquil. And more specifically with the problem of the specification of boundary wave conditions. A recurrent problem in the implementation of coastal models is the selection of proper boundary conditions. In general, users that lack directional spectral data, use constant conditions along the whole boundary domain. However, this might not be the best choice because the wave field may change significantly over the boundary. In order to offer an alternative to this problem, in this chapter, a methodology is implemented to evaluate the errors produced when constant boundary conditions are used. The aim is to provide the bases to develop a methodology based on data assimilation concepts in which single point spectra can be distributed over the whole boundary domain. In order to do this comparison, two approaches to specifying boundary conditions are compared. In the first approach, boundary conditions are set constant along the boundary. In the second, spectra are given at several points along the domain. These input boundary conditions are generated using output from a larger grid model implementation covering the whole Pacific Ocean, in this case from the WAVEWATCH III model. Apart from these scientific objectives, another important aspect has been the learning process of wave model downscaling using WAVEWATCH III and SWAN, and a major time and effort

have been dedicated to that, and it is documented here.

## 6.2 Data sources and model setup

The study area is the Gulf of Guayaquil and the bathymetric data corresponds to the free-access ETOPO1 (Amante & Eakins, 2009), presented next in Figure 6.1 in UTM coordinates.

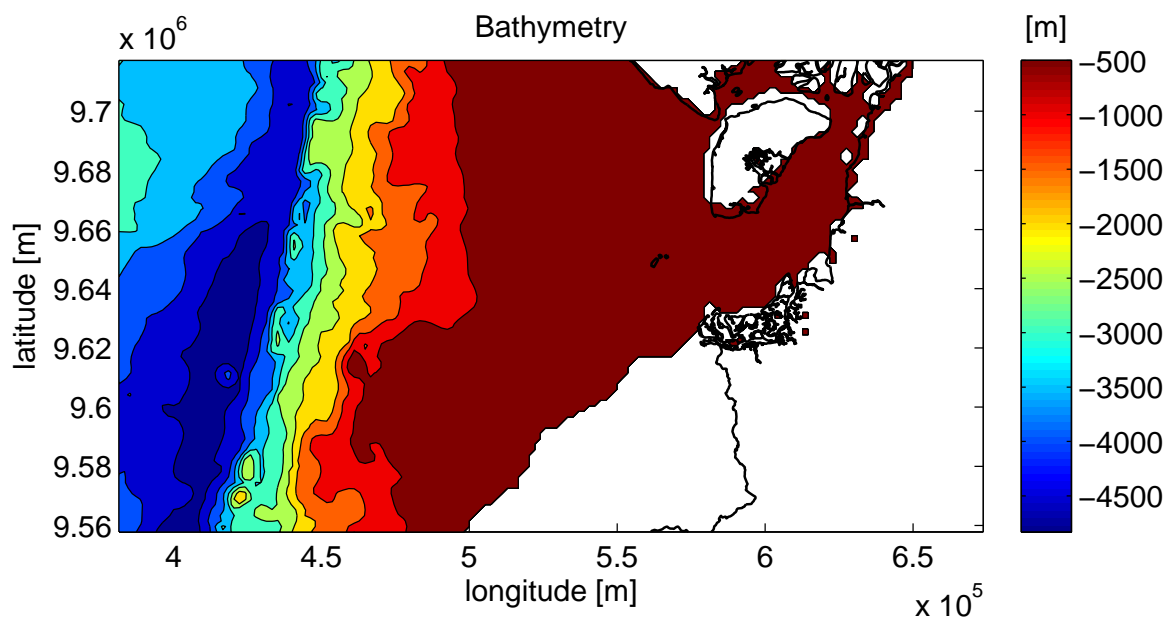
Figure 6.1a shows the water depth in meters with vertical scale showing the whole range of depths. In Figure 6.1b the contour levels emphasize the shallow water zone. It is important to note that in this region water depths range from about -4000m to 0m, in a short horizontal distance.

The model used is SWAN (Simulation WAVes Nearshore), a third-generation model specialized in shallow water environments (Booij et al., 1999). The spectral domain, is divided into 25 frequency and 180 directions. The range is between 0.03–0.3 Hz, set in geometric scale. The directions were set from 1° to 359°. The bathymetric grid is specified in UTM coordinates, and SWAN was set to use Cartesian Coordinates and it is run in stationary mode.

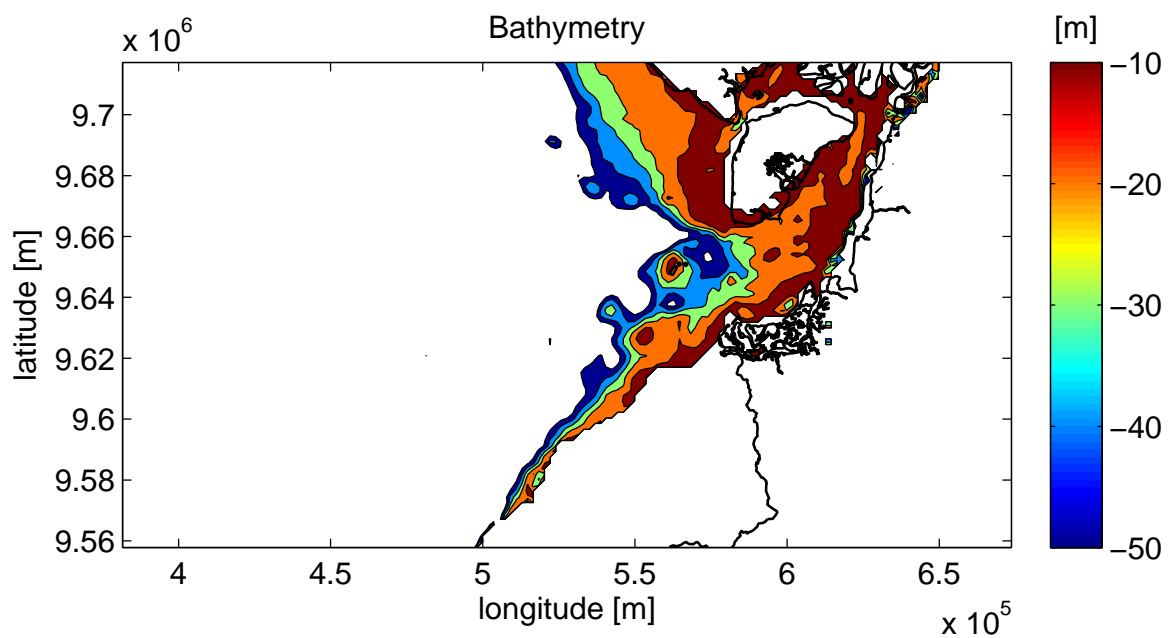
### 6.2.1 Physics

The following physical formulations were used. For more detailed information about them the user is referred to the SWAN manual SWAN Team (2014a, 2014b).

1. The GEN3 Komen package (Komen et al., 1984) to run in third-generation mode for wind input, quadruplet interactions and white-capping. The quadruplets were deactivated because in the absence of wind input this source term is weak and the SWAN model is set to switch off quadruplets when wind is not active (see for instance Rogers et al. (2007); Ris et al. (1994)).
2. Depth-induced wave breaking in shallow water (Battjes & Janssen, 1978).
3. JONSWAP bottom friction formulation (Hasselmann et al., 1973).



(a) Vertical scale adapted to show deep water areas' (UTM Coordinates)



(b) Vertical scale adapted to show shallow water areas'

Figure 6.1: Bathymetry of the study area, Gulf of Guayaquil, resolution: 1'

## 6.3 Boundary conditions

Two scenarios were run for the different boundary conditions:

1. **Constant:** Constant boundary conditions in the form of directional spectra, from a single model output point of a coarser model (WAVEWATCH III)
2. **Distributed:** Boundary conditions in the form of directional spectra, from several boundary output points of a coarser model (WAVEWATCH III).

In both cases the runs were carried out for one month, corresponding to August 2009. The coarser, larger scale model (WAVEWATCH III), was run with Wind input and Ice coverage from the ERA Interim ECMWF dataset (Dee et al., 2011) with default packages for physics (see Chapter 4). Output spectra is saved in time steps of 3-hours.

## 6.4 Results

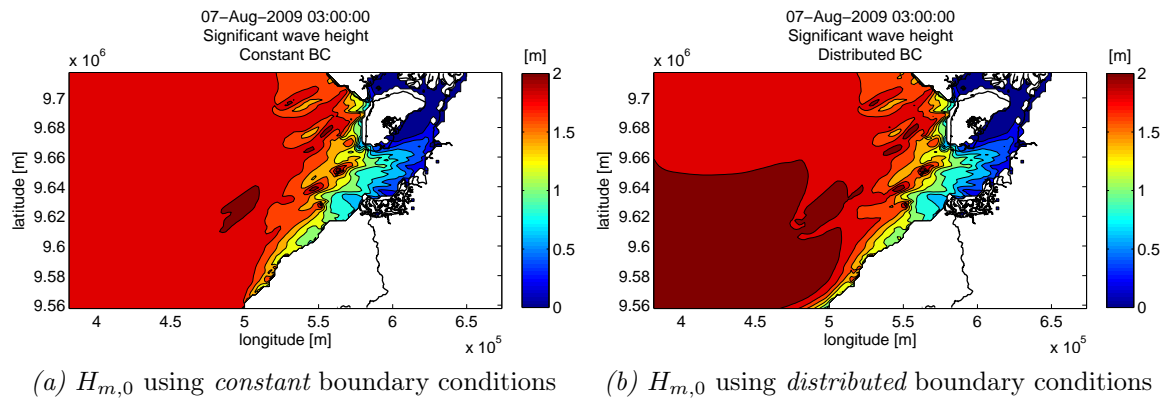


Figure 6.2: Wave field for a specific date using both approaches Constant and Distributed (UTM Coordinates)

Figure 6.2 shows the Significant wave height  $H_{m,0}$  for an evaluation run at specific date, August 7, 2009 using both approaches (i.e., Constant, Distributed). In Fig. 6.2b, there is a whole patch with values of about 2m, which correspond to only 1.7m in Fig. 6.2a. However, near the coast in the south boundary in Fig. 6.2a values of  $H_{m,0}$  are still 1.7m while in 6.2b they decay progressively to about 0.5m. These are the largest remarkable differences, in the rest of the domain, the wave conditions look

very similar. The reason might be the direction of the incoming waves and also their magnitude.

In Fig. 6.3, a time series of  $H_{m,0}$  is presented to show the magnitude of waves. In addition, a comparison was performed with data from the Era-Interim (ECMWF) at the point with coordinates  $x=5E5$  meters,  $y=9.66E6$  meters, located centrally in the domain. The figure shows in average  $H_{m,0}$  values of about 1.2m.

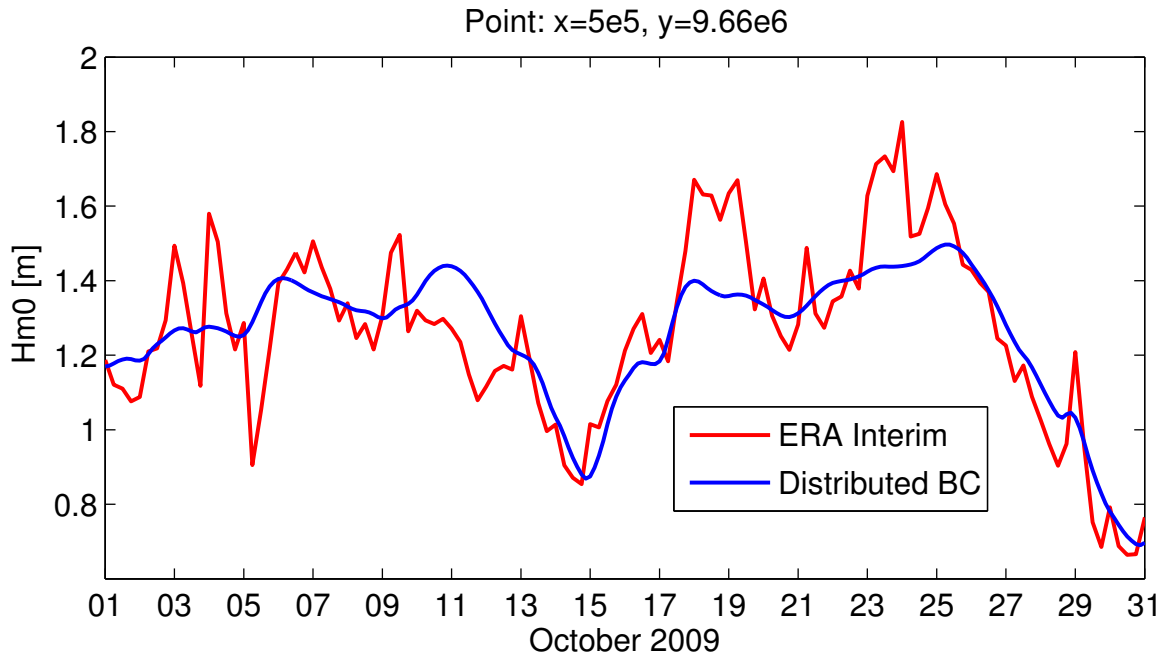


Figure 6.3: Comparison of the WAVEWATCH III run, *distributed* approach, with the ERA Interim ECMWF data.

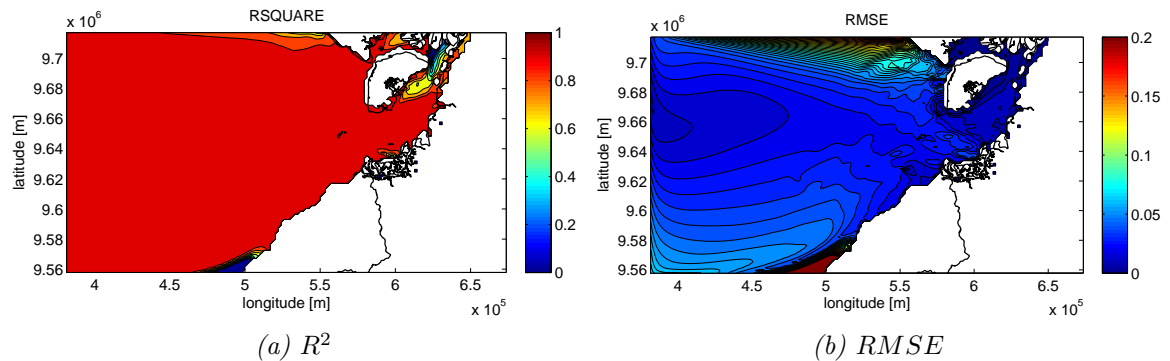


Figure 6.4: Differences in terms of  $R^2$  and  $RMSE$  evaluated for August 2009 (UTM Coordinates)

In order to evaluate the differences for the whole month, two parameters were calculated. Namely the Coefficient of determination  $R^2$  and the Root mean square



error *RMSE* Figs. 6.4a and 6.4b. There are not large differences in most of the domain, but there are specific areas where differences are large. Specifically the north and south areas near the boundaries present considerable differences with  $R^2$  values of about 0.75 and 0.10 respectively. It is important to note that behind the island low  $R^2$  values down to 0 are present. In Fig. 6.4b the magnitude of these differences ranges from 0 to 20cm. (with the largest differences of 60cm., not shown), also near the boundaries. This methodology quantifies the possible errors introduced in the model when constant boundary conditions are set. These errors are expected to be larger when wave conditions are less uniform along the boundary.

## 6.5 Summary and conclusions

The implementation of SWAN coupled to WAVEWATCH III was done successfully. On this system it was possible to evaluate the role of the boundary conditions in a regional/coastal modelling case.

Results show that in this particular case, those differences can be significant, although a period with relatively low wave conditions was considered. In addition, in this month only specific wave conditions are present, typically coming from the south (Portilla, 2011). Therefore, longer runs and also runs more specific to certain wave conditions should be carried out to evaluate the impact of BC more precisely.

# Chapter 7

## Summary and Conclusions

The wave model WAVEWATCH III was implemented successfully in the Ecuadorian Pacific following a nested multigrid approach, using a global grid, a regional grid (OPACE) and two fine grids COAST and GALAP. This model is presently used to produce wave forecasts, using wind fields and ice coverage from the NCEP-GFS databases, and it is been subject to validation.

The influence of the Antarctica sea ice extent on the Ecuadorian wave conditions was evaluated. It was found that this impact can be large in specific cases, and it can be a source of large model errors and bias. Therefore, this is an important aspect to consider for model calibration and verification. Moreover, it is noted that ice coverage information differ largely between sources, in this case between the NCEP and the ECMWF databases.

The regional scale wind wave model SWAN was implemented successfully for the Gulf of Guayaquil. It provided consistent results for the study area. The evaluated differences between two types of boundary conditions are not large, probably because of the moderate wave conditions considered. Therefore, a more detailed analysis should be made, with longer runs covering a wider range of wave conditions.

# Bibliography

- Amante, C., & Eakins, B. W. (2009). *Etopo1 1 arc-minute global relief model: procedures, data sources and analysis*. US Department of Commerce, National Oceanic and Atmospheric Administration, National Environmental Satellite, Data, and Information Service, National Geophysical Data Center, Marine Geology and Geophysics Division.
- Ardhuin, F., & Jenkins, A. D. (2006). On the interaction of surface waves and upper ocean turbulence. *Journal of physical oceanography*, *36*(3), 551–557.
- Ardhuin, F., Rogers, E., Babanin, A. V., Filipot, J.-F., Magne, R., Roland, A., . . . others (2010). Semiempirical dissipation source functions for ocean waves. part i: Definition, calibration, and validation. *Journal of Physical Oceanography*, *40*(9), 1917–1941.
- Ardhuin, F., Tournadre, J., Queffelec, P., Girard-Ardhuin, F., & Collard, F. (2011). Observation and parameterization of small icebergs: Drifting breakwaters in the southern ocean. *Ocean Modelling*, *39*(3), 405–410.
- Battjes, J. A. (1994). Shallow water wave modelling. In M. Isaacson & M. Quick (Eds.), *Proc. Int. Symp.: Waves - Physical and Numerical Modelling, Univ. of British Columbia, Vancouver* (pp. 1–23).
- Battjes, J. A., & Janssen, J. P. F. M. (1978). Energy loss and set-up due to breaking of random waves. In *Proceedings of the 16th international conference on coastal engineering* (pp. 569–587).
- Berkhoff, J. (1974). *Computation of combined refraction-diffraction*. Delft Hydraulics Laboratory.
- Booij, N., Ris, R., & Holthuijsen, L. H. (1999). A third-generation wave model for coastal regions: 1. model description and validation. *Journal of Geophysical Research: Oceans (1978–2012)*, *104*(C4), 7649–7666.
- Bouws, E., & Komen, G. J. (1983). On the balance between growth and dissipation

- in an extreme depth-limited wind-sea in the southern North Sea. *Journal of Physical Oceanography*, *13*, 1653–1658.
- Cavaleri, L., & Malanotte-Rizzoli, P. (1981). Wind wave prediction in shallow water: theory and applications. *J. Geophys. Res.*, *86*(C5).
- Chawla, A., & Tolman, H. (2007). Automated grid generation for WaveWatch III. *Technical Bulletin*, *254*.
- Collins, J. I. (1972). Prediction of shallow-water spectra. *Journal of Geophysical Research*, *77*(15), 2693–2707.
- Davis, R., & Moore, E. (1982). A numerical study of vortex shedding from rectangles. *J. Fluid Mech*, *116*(3), 475–506.
- Dee, D., Uppala, S., Simmons, A., Berrisford, P., Poli, P., Kobayashi, S., . . . others (2011). The era-interim reanalysis: Configuration and performance of the data assimilation system. *Quarterly Journal of the Royal Meteorological Society*, *137*(656), 553–597.
- Doty, B. (1995). The grid analysis and display system. *GRADS Manual*, *10*, 148.
- Ebisuzaki, W. (2006). *Simple script to download gfs files*.
- Eldeberky, Y. (1996). *Nonlinear transformations of wave spectra in the nearshore zone*. Unpublished doctoral dissertation, Delft University of Technology, Delft, The Netherlands.
- Eldeberky, Y., & Battjes, J. A. (1996). Spectral modeling of wave breaking: Application to boussinesq equations. *Journal of Geophysical Research: Oceans (1978–2012)*, *101*(C1), 1253–1264.
- Freilich, M., & Guza, R. (1984). Nonlinear effects on shoaling surface gravity waves. *Philosophical Transactions of the Royal Society of London. Series A, Mathematical and Physical Sciences*, *311*(1515), 1–41.
- Gabriel, E., Fagg, G. E., Bosilca, G., Angskun, T., Dongarra, J. J., Squyres, J. M., . . . others (2004). Open MPI: Goals, concept, and design of a next generation MPI implementation. In *Recent Advances in Parallel Virtual Machine and Message Passing Interface* (pp. 97–104). Springer.
- Gridded, E. G. (2006). *2-minute database, national geophysical data center, national oceanic and atmospheric administration, us dept. of commerce*.
- Grumbine, R. (1996). Automated passive microwave sea ice concentration analysis at ncep. *US Department of Commerce, National Ocean And Atmospheric Administration, National Weather Service, National Centers for Environmental Prediction, Technical Note, OMB contribution, 120*.

- Hasselmann, D., Bösenberg, J., Dunkel, M., Richter, K., Grünewald, M., & Carlson, H. (1986). Measurements of wave-induced pressure over surface gravity waves. In *Wave dynamics and radio probing of the ocean surface* (pp. 353–368). Springer.
- Hasselmann, K., Barnett, T., Bouws, E., Carlson, H., Cartwright, D., Enke, K., ... others (1973). Measurements of wind-wave growth and swell decay during the Joint North Sea Wave Project JONSWAP.
- Hasselmann, S., Hasselmann, K., Allender, J., & Barnett, T. (1985). Computations and parameterizations of the nonlinear energy transfer in a gravity-wave spectrum. part ii: Parameterizations of the nonlinear energy transfer for application in wave models. *Journal of Physical Oceanography*, 15(11), 1378–1391.
- Holthuijsen, L. (2007). *Waves in Oceanic and Coastal Waters*. Cambridge: Cambridge University Press.
- Janssen, P. (2004). *The interaction of ocean waves and wind*. Cambridge: Cambridge University Press.
- Komen, G., Hasselmann, K., & Hasselmann, K. (1984). On the existence of a fully developed wind-sea spectrum. *Journal of physical oceanography*, 14(8), 1271–1285.
- Komen, G. J., Cavaleri, L., Donelan, M., Hasselmann, K., Hasselmann, S., & Janssen, P. A. E. M. (1994). *Dynamics and modelling of ocean waves*. Cambridge: Cambridge University Press.
- Leonard, B. P. (1979). A stable and accurate convective modelling procedure based on quadratic upstream interpolation. *Computer methods in applied mechanics and engineering*, 19(1), 59–98.
- Leonard, B. P. (1991). The ultimate conservative difference scheme applied to unsteady one-dimensional advection. *Computer methods in applied mechanics and engineering*, 88(1), 17–74.
- Madsen, P. A., & Sørensen, O. R. (1992). A new form of the boussinesq equations with improved linear dispersion characteristics. part 2. a slowly-varying bathymetry. *Coastal Engineering*, 18(3), 183–204.
- Madsen, P. A., & Sørensen, O. R. (1993). Bound waves and triad interactions in shallow water. *Ocean Engineering*, 20(4), 359–388. doi: 10.1016/0029-8018(93)90002-y
- Miles, J. W. (1981). Hamiltonian formulations for surface waves. *Applied Scientific Research*, 37(1-2), 103–110.
- Mitsuyasu, H. (1968). On the growth of the spectrum of wind-generated waves. 1. *Rep. Res. Inst. Appl. Mech., Kyushu Univ*, 16, 251-264.

- Mitsuyasu, H. (1969). On the growth of the spectrum of wind-generated waves. 2. *Rep. Res. Inst. Appl. Mech., Kyushu Univ*, 17, 235-243.
- Moorthi, S., Pan, H.-L., & Caplan, P. (2001). *Changes to the 2001 NCEP operational MRF/AVN global analysis/forecast system*. US Department of Commerce, National Oceanic and Atmospheric Administration, National Weather Service, Office of Meteorology, Program and Plans Division.
- Padilla-Hernández, R. (2002). Numerical modelling of wind wave energy dissipation at the bottom including ambient currents. *Doctoral dissertation at KU Leuven*.
- Peregrine, D. (1967). Long waves on a beach. *Journal of Fluid Mechanics*, 27(04), 815–827.
- Phillips, O. M. (1958). The equilibrium range in the spectrum of wind-generated waves. *Journal of Fluid Mechanics*, 4(04), 426–434.
- Pierson, W. J. (1952). A unified mathematical theory for the analysis, propagation and refraction of storm generated ocean surface waves, parts {I} and {II}.
- Portilla, J. (2011). *Evaluación del recurso energético en el mar territorial ecuatoriano* (Tech. Rep. No. LOG031-11). INOCAR.
- Portilla, J. (2012). Storm-source-locating algorithm based on the dispersive nature of ocean swells. *Avances-USFQ*, 4(1), C22–C36.
- Portilla, J., Sosa, J., & Cavaleri, L. (2013). Wave energy resources: Wave climate and exploitation. *J. Renewable Energy*, 57, 594-605.
- Radder, A. (1992). An explicit hamiltonian formulation of surface waves in water of finite depth. *Journal of Fluid Mechanics*, 237, 435–455.
- Ris, R., Holthuijsen, L., & Booij, N. (1994). A spectral model for waves in the near shore zone. *Coastal Engineering Proceedings*, 1(24).
- Rogers, W. E., Kaihatu, J. M., Hsu, L., Jensen, R. E., Dykes, J. D., & Holland, K. T. (2007). Forecasting and hindcasting waves with the SWAN model in the Southern California Bight. *Coastal Engineering*, 54(1), 1–15.
- Rutledge, G. K., Alpert, J., & Ebisuzaki, W. (2006). NOMADS: A climate and weather model archive at the National Oceanic and Atmospheric Administration. *Bulletin of the American Meteorological Society*, 87(3).
- Snyder, R., Dobson, F., Elliott, J., & Long, R. (1981). Array measurements of atmospheric pressure fluctuations above surface gravity waves. *Journal of Fluid mechanics*, 102, 1–59.
- Sturm, C. (2008). *Kristof's matlab toolboxes: read\_grads*.
- Sverdrup, H. U., & Munk, W. H. (1946). Empirical and theoretical relations between

- wind, sea, and swell. *Transactions, American Geophysical Union*, 27, 823–827.
- Sverdrup, H. U., & Munk, W. H. (1947). Wind, sea, and swell: theory of relations for forecasting.
- SWAMP Group. (1985). Sea wave modelling project SWAMP. an intercomparison study of wind wave prediction models, part 1: Principal results and conclusions. *Ocean Wave Modelling*, 3–153.
- SWAN Team. (2014a). SWAN Cycle III version 41.01, Scientific and technical documentation.
- SWAN Team. (2014b). SWAN Cycle III version 41.01, User Manual.
- Teixeira, M., & Belcher, S. (2002). On the distortion of turbulence by a progressive surface wave. *Journal of Fluid Mechanics*, 458, 229–267.
- Tolman, H. L. (1991). A third-generation model for wind waves on slowly varying, unsteady, and inhomogeneous depths and currents. *Journal of Physical Oceanography*, 21(6), 782–797.
- Tolman, H. L. (1992). Effects of numerics on the physics in a third-generation wind-wave model. *J. Phys. Oceanogr.*, 22, 1095–1111.
- Tolman, H. L. (2002). Alleviating the garden sprinkler effect in wind wave models. *Ocean Modelling*, 4(3), 269–289.
- Tolman, H. L. (2003). Treatment of unresolved islands and ice in wind wave models. *Ocean Modelling*, 5(3), 219–231.
- Tolman, H. L. (2008). A mosaic approach to wind wave modeling. *Ocean Modelling*, 25(1), 35–47.
- Tolman, H. L. (2009). User manual and system documentation of WaveWatch III version 3.14. *Technical note, MMAB Contribution*(276).
- Tolman, H. L., Banner, M. L., & Kaihatu, J. M. (2013). The nopp operational wave model improvement project. *Ocean Modelling*, 70, 2–10.
- Tolman, H. L., & Chalikov, D. (1996). Source terms in a third-generation wind wave model. *J. Phys. Oceanogr.*, 26, 2497–2518.
- WAMDI Group. (1988). The wam model—a third generation ocean wave prediction model. *Journal of Physical Oceanography*, 18(12), 1775–1810.
- Wessel, P., & Smith, W. H. (1996). A global, self-consistent, hierarchical, high-resolution shoreline database. *Journal of Geophysical Research: Solid Earth* (1978–2012), 101(B4), 8741–8743.
- WISE Group. (2007). Wave modelling—the state of the art. *Progress in Oceanography*, 75(4), 603–674.

Young, I. R. (1999). *Wind generated ocean waves*. Oxford: Elsevier Science.